Deep Levels In N-Type Silicon Induced By MeV He^+ Ions

A Thesis Submitted

in Partial Fulfillment of the Requirements

for the Degree of

Master of Technology

by

Rajnish Kumar Gupta

to the

MATERIALS SCIENCE PROGRAMME

INDIAN INSTITUTE OF TECHNOLOGY, KANPUR

January ,1997

MSP-1997-M-GUP-DEE

CERTIFICATE

It is to certify that the work contained in the thesis entitled *" Deep Levels in N-Type Silicon Induced by MeV He^+ Ions "* by Rajnish Kumar Gupta, has been carried out under our supervision and has not been submitted elsewhere for a degree.

(Dr. Y. N. Mohapatra)
Materials Science Programme
Indian Institute of Technology
Kanpur - 208 016

(Dr. V. N. Kulkarni)
Department of Physics
Indian Institute of Technology
Kanpur - 208 016

January , 1997

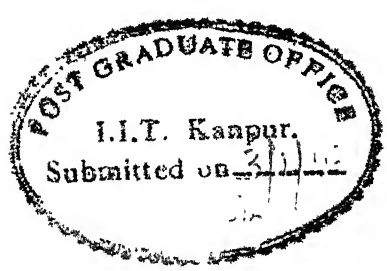

To

DEEPA

ACKNOWLEDGEMENTS

I am sincerely grateful to my thesis supervisors who guided me throughout this programme with patience and understanding. I express my sincere gratitude to Dr. Yashowanta N. Mohapatra who introduced me to this field and helped me in strengthening conceptual foundations ; and Dr. Vishwas N. Kulkarni who introduced me to the world of ion beam studies.

I am grateful to Dr. J. Narayan for professional help during my experiments. I am also obliged to my lab seniors, Sankar for initiating me to experiments, Giri for experimental guidance and Tapo for lucid introduction to principle behind various equipment used in the laboratory.

I am thankful to my friends who assisted me during my experiment and made my stay enjoyable at IIT Kanpur, J.Singh, Manoj, Girdhar, Tayyab, Sanjiv, Lakhmani, Puthal and Rajesh along with Nigam, Sharma, Purwar, Vishnu, Sangeet, MPA, who shared the memories of my earlier institution.

My thanks to Mr.M.M.Gupta, Mr.K.Masood, Mr. Rajput and Mr. Shivprakash for help during my experiments and staff of ACMS and Physics Workshop for job preparation.

Finally, I cannot forget emotional and moral support from my parents, sister and brothers during the period when it was most needed.

ABSTRACT

The study of damage and electrically active traps induced by He^+ ions in semiconductors is important from both fundamental and application point of view. In this work electrically active defects induced by high energy He^+ in n-Si have been studied using capacitance transient spectroscopy. The He^+ irradiations were performed at an angle so that the range of the particle is well within the limits that can be probed by standard capacitance spectroscopic methods. The damage profile was studied by TRIM92 simulation. The spectroscopic methods such as TSCAP, DLTS, TATS were used after irradiations into a pre-fabricated Schottky diode. Preliminary sample characterization using I-V and C-V techniques were also carried out. The energy of the He^+ ions was chosen to be 1.3 MeV. The samples were irradiated at an angle of 65° with respect to the surface normal. The doses were between 10^{12} to 10^{13} /cm^2.

Three major peaks are detected in DLTS spectra of irradiated samples. The peaks corresponding to energies 0.23eV and 0.41eV are identified to be due to two different charge states of divacancy V_2 in silicon. A majority carrier high temperature peak of large concentration has been observed to occur for the first time in α-irradiated samples. Though the energy of this peak is relatively low at Ec-0.28eV, it appears at higher temperature due to its low electron capture cross-section. On the basis of capture cross-section this level appears be a repulsive centres for

electrons. The concentration of the $V_2(=/-)$ peak at Ec-0.23eV is found to be smaller than the corresponding $V_2(-/0)$ peak at Ec-0.41eV level. This is most probably due to larger strain caused by high dose implants. There are other unidentified traps whose occurance was dependent on the dose. The traps identified were all point defects and did not show any broadening in energy level though doses of 10^{12}-$10^{13}/cm^2$ were used to create damage. The point defect nature was concluded from careful analysis of DLTSlineshapes. The defct profile of divacancy level is experimentlly obtained from variable filling pulse-width DLTS measurements, and was compared with vacancy distribution obtained from TRIM92. The depth obtained from space charge widths turns out to be apperant depth, and a model is proposed to explain observed differences. The FWHM of depth profile of vacancies predicted by simulation is in good agreement with the profile obtained for divacancy level V_2.

This work demonstrates several advantages of using oblique incidence geometry in inducing damage and deep level defects by MeV α-particles in n-type silicon. The advantages accrue from the fact that range of ions can be limited without sacrificing the use of high energy and high dose to produce large number of defects. The work has also fulfilled the goal of developing a clean method to create controlled amount of well-characterized point defects for purposes of in-house calibration in semiconductor laboratory at IIT Kanpur.

Contents

List of Figures

LIST OF TABLES

CHAPTER 1

INTRODUCTION

The study of defects in semiconductors induced by high energy radiation continues to be one of the fascinating areas of research for both fundamental reasons and applications. As a matter of fact radiation induced defects in semiconductors has become a field by itself [1]. The motivations behind these have been primarily to

(i) understand and control undesired defects due to radiation in semiconductor devices such as Schottky barriers and MOS devices used in space, and those in the environment of high energy particles,

(ii) introduce controlled amount of defects in specific regions of the device to tailor the lifetime of carriers as in striped semiconductor lasers, power devices and isolation in GaAs technology;

(iii) control and remove defects produced during ion implantation of dopants and creation of buried layers;

(iv) create controlled amount of point defects in clean environment for fundamental studies.

Majority of the reported studies have utilized energetic electron or proton beams[2]. It is only recently that irradiation studies using high energy heavier projectiles are becoming interesting from the point of view of applications.The technological possibilities of using high energy ion beams to produce buried oxide layers, retrograde wells or burried junction etc.are being intensly studied in 90s[3-5]. As a result there is renewed interest in identifying and understanding defects created by high energy ions. The success of any technology based on high energy ions would ultimately depend on the ability to control associated damage related defects. Hence, there has been intense activity as regards defect characterization in terms of identification, production rate, dose and energy dependence and annealing kinetics. The use of capacitance spectroscopies using depletion layers,such as deep level transient spectroscopy (DLTS) for characterization of defects has accelerated the progress in understanding of irradiation induced defects in semiconductors[2].

The studies based on high energy He^+ ions in semiconductors are relatively few. Mostly these studies have been in the context of particle detectors. Alpha particle radiation studies provide connection between defects produced by light particles such as electrons and protons on one hand and heavier ions on the other. These studies are

also important in isolating chemical effects of hydrogen in the target material from those purely due to inert species such as helium[2,6].

There has also been interest in the role of alpha particle radiation in producing electron-hole pairs in small geometry devices[7]. For example, the passage of alpha particles through a memory array area in charge couple devices and dynamic random access memory can create enough electron hole pairs near a storage node to cause a random, single-bit error. This is commonly known as "soft error " in VLSI memory circuits [7] On the other hand there is also an effect called as "hard error" in which degradation of data holding characteristic of memory cells occur by permanent junction leakage caused by high energy irradiations. It is interesting to note that Takuchi et al [8] have shown that aplha particles produced by radioactive decay of uranium and thorium which are present in parts per million levels in packaging materials can cause such errors.

Most of the work on high energy He^+ induced defects in silicon has been done using high resistive bulk silicon, since the range of He^+ ions having energy of few MeV is greater than few tens of microns[9]. It is for this reason that none of the studies use epitaxial silicon layers since typically these layers are only few microns thick. Also, most of the studies so far have used low irradiation

fluences to produce defects[6,10,11]. In this work we study electrically active point defects induced by high dose (> 10^{12} ions/cm^2) He^+ ions in device grade epitaxial silicon by limiting the range of ions by using oblique incidence geometry while implanting. We have used defect specific capacitance spectroscopies such as DLTS, thermally stimulated capacitance (TSCAP) and related techniques to characterize deep level defects induced in n-type silicon.

Before we state our problem more precisely, we first give a brief introduction to deep level defects along with a short review of He^+ induced defect studies in silicon.

2 Deep Level Defects in Semiconductors:

Point defects produced either by incorporation of impurities or due to intrinsic defects such as vacancies, interstitial and their complexes introduce energy states in otherwise forbidden energy gap of a perfect semiconductor. If the activation energy for the carrier release from such a level is more than hundred meV or so, the corresponding defects are termed as deep level defects[12,14]. They arise due to short range defect potential in contrast to long range Coulombic potential produced by substitutional dopants such as boron or phosphorus in silicon[15]. The deep defect levels control carrier traffic between the bands and hence

determine carrier lifetime in semiconductors.

Characterization of such deep levels would normally involve finding activation energy for carrier release (E_T), capture cross-section (σ_n), concentration (N_T), and their depth distribution in sample[12,15]. These parameters are most conveniently obtained from measurement of emission rate of carriers from occupied traps. The emission rate of electrons e_n is given from the principle of detailed balance by

$$e_n = N_c < v_{th} > \sigma_n \exp(-E/k_B T)$$

where N_c is the effective density of states of conduction band, $< v_{th} >$ the average thermal velocity, k_B is Boltzmann constant and T is temperature.

The monitoring of change in charge state of defect levels is best done through measurement of change in capacitance of a depletion layer in which the defects are present. In methods utilizing depletion layers, the occupation of the defects are controlled by electrical pulsing of the space charge layer. Hence a non-equilibrium occupancy can be easily forced. The return of the occupancy to equilibrium is monitored by measuring depletion layer capacitance as a function of time, thus enabling determination of rate of carrier emission from defect states. This principle is at the heart of all transient spectroscopies based on

capacitance[16]. The strength of the decaying signal has information regarding concentration of traps. The profile of defect concentrations can be obtained by varying the region being probed conveniently through changes in depletion layer width, which is controlled by voltage applied to the diode under test. The details of the methods of signal processing and analysis needed to obtain the relevant parameters are described in Chapter 3.

.3 Defects Induced by He^+ ions : A Brief Review

It is well known that bombardment of silicon with ions introduces defect states in the energy gap. If the ion is electrically and chemically inactive as is He in silicon, one expects only damage related defects caused by primary or secondary displacement cascades. Early work on alpha particle irradiation was done primarily to compare effects due to electron and proton irradiation with that of He^+[6]. In late seventies Kimerling[6] showed that the point defect character predominates even when silicon is bombarded with MeV alpha particles. Since then several workers[17,10,11] have tried to catalogue the list point defects produced by alpha particles through their electrical signature controlled by energy and capature cross-section.

Irradiation of silicon with high energy particles, in general, results in creation of defects such as vacancies and interstitials, which are unstable at room temperature and are observed only as defect complexes[2]. The divancancy (V_2), A centre (oxygen-vacancy complex) and E centre

(donor-vacancy complex) are the well identified defect complexes commonly observed in various studies in n-silicon. The microscopic structures of these complexes have been studied by EPR [18], optical and electrical properties are determined by IR [19] and DLTS [6,10-11,17].

The reports by Kimerling[6], and Berman et al [20] were by defects created by very low dose of α-particles ($<10^{11}/cm^2$). In fact, this feature of low dose is common to almost all studies. The report by Indusekhar et al [17] had used very high fluences but the energy used was 30 MeV so that the particles escaped the silicon samples after traversing full thickness. Hence though they used large doses, the effective introduction rate of defects was small yielding results comparable to low doses. Therefore most of the studies report only small concentration of defects produced and use low background doping to increase sensitivity of detection.

As in case of most ion-irradiated n-type silicon, DLTS reveals three dominant defect levels at Ec-0.17 eV, Ec-0.21 eV and Ec-0.41 eV. The level at Ec-0.17 eV has commonly been attributed to oxygen-vacancy pair. It behaves as an acceptor type defect and its introduction rate is dependent on oxygen content in the sample [2,6]. In crucible grown crystals, the oxygen incorporated during growth produces large amount of this centre. Even for float zone material, it has been shown [6] that the oxygen incorporation during device fabrication steps is enough to give detectable levels of

A-centre. A characteristic of this centre is that it can be annealed out at 400 C, though its stabilization by forming complexes at higher temperatures have been reported at much higher temperatures.

The defect levels at Ec-0.23 eV and Ec-0.41 eV have been attributed to different charge states of the divacancy[2]. The former is associated with transition from double negative charge state to singly charged state, and the latter one with a furhter emission of an electron to become neutral. Recently this correlation has been studied in more detail by Svensson et al[11]. They have compared DLTS signal heights corresponding to these two levels after introducing them by set of different energetic particles viz. electrons, He, O and Br. They show that in electron-irradiated sample the concentrations are almost equal while for heavier projectiles the Ec-0.41 eV peak increases gradually with increasing ion mass. This is attributed to the fact that V_2 centres are formed by heavy ion bombardment occur in lattice regions which accommodate a larger strain that for light ion bombardment. They also argue that that the Ec-0.41 level broadens in energy due to the same reason. However the lack of one to one correspondence between the two charged states of the defect is controversial [11,21] and coherent explanation is yet to be found. Svensson et al [11] propose that it is due to motional averaging of two different configurations of the defect. Further, the identification of Ec-0.41 eV is

sometimes attributed to another defect due to donor-vacancy complex[2]. There have been reports of additional defect levels without nailing down their origin. [17,22]. Their occurrence seem to depend on dose, introduction rate and the quality of the starting material. Hence their has been differences in the energy spectrum reported by different workers.

The depth profile of defects produced by high energy He^+ ions have been critically studied by Palmetshofer and Reisinger[10].They compared the profiles obtained with H^+ and D^+ ions.They show that α-particle irradiation causes only pure defect levels whereas H^+ and D^+ implantation cause additional hydrogen related defects. Interestingly they observed donor dependence of width of depth profiles and argue that profiles broader than theoretically expected occur due to electric field enhanced diffusion. According to their argument such broadened profiles would not occur if irradiations are done within the depletion layer of a Schottky barrier or diode.

In summary, it can be said that standard vacancy related defects appearing due to low fluences of α-particles are fairly well known. However there is a lack of studies with high dose and in epitaxial layers. The other damage related levels have not been even properly identified and thus much less understood.

.4 Statement of the problem:

The primary goal of this work is to characterize

defects induced in n-silicon using high fluences so of α-particles.This is to enable creation of large and controlled amount of defects at a desired depth using He^+ ions. The range of a typical MeV He^+ ions in silicon is normally very large (eg 5MeV α-particle has a range of 22um). For most device work buried layers are needed only few microns below the surface. Therefore we propose to limit the range of the incident particles to the desired depth by carrying out irradiation at a precalculated angle of incidence of the ion beam on the sample. This has also the advantage of being able to keep the induced damage and defects within the top device grade epitaxial layer which is typically a few microns thick. Since the need to use large depletion widths is not required for characterization in such a case, we can use samples with realistic doping levels. This is in contrast to the use of high resistivity silicon samples by most other workers. Also, limiting the range of the ion beam by oblique incidence geometry enables defect characterization using Schottky barrier diode configuration which involves simpler processing steps and would not cause defect profile broadening as pointed out by Palmetshofer and Reisinger[10]. In addition this would enable us to use high doses of irradiation which in turn facilitates study of large concentrations of defects without sacrificing sensitivity of detection of capacitance based characterization methods.

Since there are so many advantages of defect

production using oblique angle incidence, our primary goal in this work is to demonstrate its feasibility using α-particles. This work is limited to n-type samples. The energy of α-particles is chosen to be 1.3 MeV and dose of the order of 10^{12}-$10^{13}/cm^2$. Most previous works use doses less than $10^{10}/cm^2$. The induced defects in pre-fabricated Schottky diodes are characterized using current-voltage, capacitance-voltage and capacitance spectroscopies such as DLTS and TSCAP. The damage parameters are simulated using TRIM92[9]. The predicted depth profiles of vacancies from TRIM92 are compared with experimental profiles for vacancy related defects.

This work was also motivated by the need to develop a standard clean method of creating controlled amount of well characterized point defects for in-house calibration purposes in the semiconductor materials laboratory of the Institute.

CHAPTER 2

EXPERIMENTS AND TECHNIQUES: Sample Preparation

This chapter gives a brief description of experimental procedures and arrangements involved in the study of deep level defects.

2.1 SAMPLE PREPARATION

2.1.1 CLEANING PROCEDURES FOR SAMPLES

Experiments involving movements of atomic species are highly influenced by the presence of foreign atoms and hence it is essential to prepare as clean a sample as possible. Before the deposition of Au for schottky contact and Al for ohmic contact, the substrates were etched to remove the surface contaminants (mainly oxides).

The cleaning steps described below[22]

De-greasing:

In the first step the substrates are cleaned using organic solvents such as trichloroethylene(TCE) followed by thorough rinse in Acetone.

Etching:

Etching of Silicon substrate is carried out by a brief stirring of the wafers in a etching solution of 1:50 HF:H_2O(distilled) for 30 seconds. This is a planar etch with an etch rate of 5 μm/min.Immediately after etching the sample was cleaned in deionized water to remove residues

for further etching. This process was repeated till shining surface was obtained indicating the removal of oxide.

RCA Cleaning:

This cleaning was final step before deposition . This process is commonly followed by semiconductor industry and was performed on the wafers which are mechanically polished. It consist of the following steps.

* A ten min. boil in 1:1:5 solution of NH_4OH : H_2O_2 : H_2O
* A ten min. boil in 1:1:5 solution of HCl : H_2O_2 : H_2O
* A 30 sec. dip in 1:50 of HF : H_2O
* A through rinse in de-ionized water and then dried.

2.1.2 THIN FILM DEPOSITION

Aluminium thin film was deposited by thermal evaporation unit.

Thermal Evaporation:

Al film of thickness 2000A was deposited in a clean and high vacuum of order 10^{-6} torr using Tungsten boat.

Here the mass of Al (M) required to obtain a film of thickness (t) was calculated on the basis of following relation[23].

$$M=2\pi R^2 \rho t$$

Where ρ is the bulk density of Al to be evaporated and R is the distance between substrate and boat.

The evaporation was carried out under 2π geometry ie under the assumption that the vapors diffuse in a solid angle of 2π Fig2.1(a).

Electron Beam Evaporation:

Au films of thickness 1000A were deposited under e-beam in a clean vacuum of 10^{-6} torr with the Au pieces of high purity place in graphite crucibles[24]. The working principle of e-beam apparatus involves the generation of thermoionic electrons from a tungsten filament and the bending of these electrons towards graphite crucible which contain the material to be deposited.While the thermoionic electrons are generated by passing current through tungsten filament,the bending obtained by permanent magnate and high -ve voltage Fig 2.1(b).

The major advantage of e beam evaporation over thermal evaporation are accurate control of rate of deposition which is an important parameter associated with film adherence,no requirement to measure the mass of substrate accurately , and the ability to perform a number of evaporation of different materials without breaking the vacuum since there is also a facility for multiple evaporation using rotating crucibles. The rate of deposition can be controlled by the current passing through the Tungsten filament providing the thermoionic electrons.

2.2 He^+ ION IRRADIATION:

He^+ ions of energy 1.3 MeV generated by the Van de Graaff accelerator was used to irradiate the sample with dose of 10^{11}-10^{14}ions/cm. The beam spot on the sample was typically of $4mm^2$ as measured on paper.The irradiation was carried out at room temperature and vacuum of order 10^{-6} torr. This section describes the He^+ irradiation port used

for room temperature[22].

He^+ Ion Irradiation Port:

Associated Fig 2.2 gives the details of He^+irradiation port. This chamber is mounted on a diffusion pump vacuum system with a liquid nitrogen trap which yields a vacuum of order $1.0*10^{-6}$torr. This vacuum is quite adequate for irradiation work.With this care taken ,carbon deposition can be avoided on the sample during irradiations.

The sample was mounted on a sample holder (electrically isolated from the grounded chamber). On the facing side of beam .a quartz crystal is placed. The quartz plate gives out a blue glow when ion beam falls on it. The purpose of this arrangement is to aid in the alignment of ion beam.

Surrounding the sample holder there is a cylinder made of aluminum sheet which has an opening for the passage of ions. This cylinder is maintained at a potential of -260 V relative to grounded chamber. This arrangement is called a suppressor which inhibits the emission of secondary electrons from the sample during ion irradiation. In the absence of such a suppressor the secondary electron emission can interfere in the measurement of total charge during ion irradiation.

The beam which centers the chamber is collimated by X-Y slits.By the time it reaches the chamber it spreads slightly and is further collimated by an aperture,mounted just before the sample holder. The aperture can be adjusted

for area up to 5*5 mm^2. In the irradiation carried out the ion current density used have been 0.2$\mu A/cm^2$.

A movable sample holder used in irradiation port enable us to analyze or irradiate several samples without breaking vacuum. The holder is electrically isolated from the rest of the chamber by a perspex flange. A current integrator is connected to the sample holder. It measures the total charge acquired during the irradiation. From the collected charge the dose(number of ion per cm^2) is calculated.

Sample holder is mounted on a calibrated angle scale, this adds the facility for irradiation at an angle between 0^0 and 180^0. In this experiment angle adjusted to 65^0.

2.3 MeV ION FACILITY:

The 2MeV Van de Graaff facility has been utilized in this work.The accelerator has been described in detail by Banerjee N.[25] and schematic layout of ion beam irrdiation facility shown in Fig 2.3.

CHAPTER 3

EXPERIMENTS AND TECHNIQUES:

Electrical Characterization

3.1 Current-Voltage Characteristics:

3.1.1 Theory:

The ideal current voltage characteristics are based on the following four assumptions[26]: (1)the abrupt depletion layer approximation; ie the built in potential and applied voltage,are supported by a dipole layer with abrupt boundaries, and outside the boundaries the semiconductor is assumed to be neutral; (2)the Boltzman approximation; (3)low injection of minority carrier compared to majority carrier; (4)no generation carrier exists in the depletion layer and electron and hole currents are constant through the depletion layer. The total current given by :

$$J=J_p+J_n = J_s(e^{qv/kT}-1)$$

$$J_s=(qD_p p_{no})/L_p+(qD_n n_{po})/L_n$$

This equation is celebrated as Schottky equation, which gives the qualitative ideal current-voltage characteristic of Schottky diode. The departure from the ideal are mainly due to : (1)the surface effect,(2)the generation and recombination carriers in the depletion layer, (3)the tunneling of carriers between states in the band gap, (4)the high injection condition that may occur even at relatively small forward bias, (5)the series resistance effect. In addition , under sufficiently larger field in the reverse direction, the junction will breakdown. The ideal current

vs. voltage characteristic shown in Fig.3.1(b)

3.1.2 INSTRUMENTAL DETAILS:

Sample shown in Fig.3.1(b) was mounted inside a conical shaped aluminum cryostat which has a Copper-Constantene thermocouple(linear output signal between $80^{\circ}K$-$350^{\circ}K$). A heater wire 30 V, 150Ω is connected to it for raising the temperature near $300^{\circ}C$ and water-ice mixture is used as constant temperature reference point.

Power supply to heater is given by model 3161,30V,150W source. Keithly 485 ammeter with 0-2nA-2mA range and resolution of 0.1pA is used for measurement for current. The maximum limit of input voltage is 50 V for 20μA-2mA range and 350 V for rest. This ammeter operates satisfactory in $18^{\circ}C$-$28^{\circ}C$ temperature range.

This ammeter is connected to PC 286/AT with 4853 IEEE-488bus which is also receives the digital data of temperature of sample from Keithly 197 voltmeter.

Keithly 197A is used for measuring applied voltage to sample and sending current and voltage values to PC286/AT. It has input impedance of 1MΩ and 47pF.Maximum voltage of 250 V(pp) can applied to this. It has frequency of 1MHz for 8bit and 100kHz for 16 bit sampling.It has 14 digit alphanumeric display with mathematical,filtering and zero setting operation. Schematic diagram of measurement set-up shown in Fig.3.1(c).

3.1.3 Interpretation:

In ideal condition current voltage characteristic of damaged sample should be nearly same as virgin sample

characteristic. This imply that carrier density is not effected by high energy ion damage, hence damaged sample can be used for further measurement.

3.2 Capacitance-Voltage Characteristic:

3.1.1 Theory:

Although the carrier concentration is related to the resistivity, it is usually not derived from resistivity measurement but it is measured independently. One of this method is Capacitance-Voltage profiling[27].

A depletion layer as shown in Fig.3.2(a) establish due to the built-in(V_b) voltage and applied (V_a)voltage and electron density distribution can be given by n(x) at the edge of depletion region. Charge distribution can be given by electron in metal and positive charge in semiconductor as

$d^2\psi/dx^2=-\rho(x)/\varepsilon\varepsilon_o$ where $\rho(x)$ is the charge distribution profile. In metal charge is small compared to semiconductor hence solution of above equation can be given by

$\psi(x)=((x_d-x)^2eN_d)/(2\varepsilon\varepsilon_o)$ here x_d is the depletion layer width and electron distribution in vicinity of this region can be given by

$$n(x)=N_d\exp[-(x_d-x)^2/2L_d^2]^{1/2}$$

$L_d=(\varepsilon\varepsilon_o kT/e^2N_d)$ this distance is called Debye length.

depletion region capacitance is given by $C=AdQ/dV$ in $dV=dV_a$ because V_b is almost constant. The term dQ arises from

(1)fluctuation of electronic charge in vicinity of edge x_d

causing fluctuation in $e(N_d(x)-n(x))$

(2) another contribution on charge in donar line in vicinity of x_1 where it cross E_F.

(3) state at interface x=0 also contribute fluctuation and dominant in insulating interfacial layer.

for simple derivation we assume that $L_d << x_d$ ($V >> kT/e$) and divided sample in (1) space charge region , (2) interior region which is everywhere neutral, (3) abrupt change at x_d.

Capacitance measurement is also influenced by frequency N_t/N_d and series resistance. For 1.0% error series resistance should be less than $0.1(\omega_1 C)^{-1}$.

Capacitance-Voltage Profiling: Assuming the case of ideal capacitor and depletion approximation x_d is well defined, provided there is no influence of deep states. With this assumptions the depletion depth increases by Δx_d when the bias is increased by ΔV doping concentration can be given by

$N(x_d) = -(C^3/(e\varepsilon\varepsilon_0 A^2))(\Delta C/\Delta V)^{-1}$ so that the measurement of C and $\Delta C/\Delta V$ as function of V gives $N(x_d)$ as a function of x_d. This curve shown in Fig.3.2(b).

This method of non destructive profiling is limited by (1) fundamental, (2) instrumental, (3) sample limitation.

Maximum depth in a sample is limited by reverse breakdown field which gives higher depth for lower doped sample. Depth resolution can be represented by $\simeq x_d \pm 2L_d$ further difficulties arise due to the diffusion of free carrier, gradient of concentration, established charged dipole within undepleted material and as the depletion layer

of the surface contact approaches redistribution of charge occur.

The profiling instrument determines the accuracy with which $N(x_d)$ and x_d are measured and may also determine the depth resolution; ideally, the depth resolution should be limited by the Debye length rather than instrument. From mathematical analysis it can be seen that it is difficult to achieve a satisfactory balance between optimum depth resolution and accuracy in the measurement of N in depletion profiling and this arises from coupling between $\Delta x_d, N(x_d)$ and depth.

Distortion may be introduced in a C-V profile by deep states in the material and by series resistance and leakage in the test diode.

3.2.2 Instrumental Details:

A Boontan 72B capacitance meter is used which has 1,3 10,30,100,300,1000,3000 pF ranges. Its resolution is 0.5% and frequency of crystal is 1Mhz.Maximum bias voltage that can be applied is ±600 V.

Other instruments used are same as in section 3.1.2 and schematic diagram of its experimental set-up shown in Fig.3.2(c).

3.2.3 Interpretation:

Differential C-V profiling is more useful technique for determining doping concentration as function of depth,freezing characteristic(by determining carrier concentration at various temperatures) and also in transient study.

3.3 Transient Techniques:

3.3.1 Theory:

The energy level and concentration of deep level impurities can be best measured electrically by transient study at various temperatures[28].

Generation-Recombination Statistics:

A band diagram of perfect crystal consist of a valence band and conduction band separated by band gap. When periodicity of the single crystal is perturbed by foreign atoms or crystal defects, discrete energy levels are introduced into the band gap. Each centre with energy E_T is known as trap level or generation-recombination centre. Each of these centers can either capture/emit electron to conduction band or capture/emit hole to valence band as shown in Fig.3.3(a). If capture of electron from conduction band followed by emission of electron to conduction band then it is called trapping and if capture of electron from conduction band followed by capture of hole from valence band then it is called recombination centre. In generation centre emission of electron to conduction followed by emission of hole to valence band.

Above process can be given in mathematical form

$N_T=n_T+p_T$ where N_T is the concentration G-R centres

n_T is the concentration of G-R centres occupied by electrons.

p_T is the concentration of G-R centres occupied by holes.

$dn/dt|_{G-R} = e_n n_T - c_n n p_T$ and

$dp/dt|_{G-R} = e_p p_T - c_p p n_T$ where e_n, e_p are emission rates

p,n are concentration of holes in valence band electrons in conduction band.

The solution of above equation can be given by

$n_T(t) = n_T(0)e^{-t/\tau} + ((e_p+c_n n)/(e_n+c_n n+e_p+c_p p))N_T(1-e^{-t/\tau})$ and

steady state concentration by

$n_T = ((e_p+c_n n)/(e_n+c_n n+e_p+c_p p))N_T$ by assuming (1)p negligible, (2)n spatially homogeneous i.e.n(t) is exponential. Above equation can be simplified to

$n_T(t) = n_T(0)\exp(-t/\tau_e) \simeq N_T\exp(-t/\tau_e)$

The steady state G-R centre concentration n_T in the reverse biased scr region is

$n_T = (e_p/(e_n+e_p))N_T$ when diode is pulsed from reverse bias to zero bias, electrons rush in to be captured by G-R centres in p_T state. The dependence of n_T during the capture period is

$n(t) = N_T - [N_T - n_T(0)]\exp(-t/\tau_c)$ where $\tau_c = 1/c_n n$.

Transient Measurement:

It is obvious from transient equations that scr changes as electrons are emitted from G-R centres and this is detected as time-varying capacitance as shown in Fig.3.3(b) and its equation is

$\Delta = ((qK_s\varepsilon_o N_D)/2(V_{bi}-V))^{1/2}(1-(n_t(t)/N_D)^{1/2}$

$\simeq 1-n_T(t)/2N_D)$

majority carrier emission capacitance increases with whether impurity is donor or accepter type and of detailed balance also fulfilled in equilibrium

Under assumption emission and capture time

constant remain equal to their equilibrium values under non-equilibrium conditions. We obtain the emission time constant as

$\tau_e = (\exp[(E_C - E_T)/kT])/\sigma_n v_{th} n_1$ similar equation can be derived for holes. Its another form is

$\tau_e T^2 = \exp[(E_C - E_T)/kT]/\gamma_n \sigma_n$ γ_n is constant, σ_n is capture cross section.

For majority carrier capture, analysis can be done when diode is switched to zero bias from sufficiently long time in reverse bias condition. The concentration of G-R centres able to capture majority carrier , for negligible emission , is given by

$n_T(t_f) = N_T - [N_T - n_T(0)]\exp(-t_f/\tau_c)$ t_f is called filling time and this controls the concentration of G-R centres occupied by electrons. This relation can be given by

$\ln(\Delta C_c) = \ln\{[N_T - n_T(0)]/2N_D\} - t_f/\tau_c$ where $\Delta C_c = C(t_f) - C(t_{f=\infty})$

A plot of ΔC_c vs t_f has a slope of $-1/\tau_c = -\sigma_n v_{th} n$ and intercept gives trap concentration.

Deep Level Transient Spectroscopy:

If the C-t curve from a transient capacitance experiment is processed so that a selected decay rate produces a maximum output, then a signal whose decay time changes monotonically with time reaches a peak when the rate passes through the rate window of a boxcar averager or the frequency of lock in amplifier. When observing a repetitive C-t transient through such rate window while varying the decay time constant by varying the sample temperature, a peak appear in the temperature Vs output plot is named as a

DLTS spectrum. This peak is shown in Fig.3.3(c).

In Boxcar DLTS technique C-t waveform are sampled or gated at times t_1 and t_2 and capacitance $C(t_2)$ is subtracted from $C(t_1)$ this difference passes through maximum at some temperature T_1.The DLTS signal obtained by weighting function $w(t)=\delta(t-t_1)-\delta(t-t_2)$ in

$\delta C=(1/T)\int_0^T f(t)w(t)dt$ $f(t)$ is capacitance signal

at temperature T_1 $\tau_{e,max}$ is given by

$\tau_{e,max}=(t_2-t_1)/(\ln(t_2/t_1))$ this is independent of magnitude of capacitance and the baseline of the signal need not be known. Setting of t_1 and t_2 can be done by(1) t_1 fixed,vary t_2,(2) t_2 fixed t_1 vary,(3) t_2/t_1 fixed vary t_2,t_1.Last is preferred to earlier because magnitude remain same in size and shape.

It has been experimentally found that the sampling or gate width should be relatively wide because signal/noise ratio proportional to the square root of gate width.Impurity concentration cannot be determined from DLTS signal because this does not give capacitance step.Trap concentration is given by

$N_T=(\delta C_{max}/C_0)2N_d(r^{r/(r-1)}/(1-r))$ where $r=t_2/t_1$.

3.3.2 Instrumental Details:

Schematic diagram of this measurement system is given in Fig3.3(d). Capacitance meter has already described in section (3.2.2) and other instrument has described in section (3.1.2). In computer DLTS system entire waveform can be obtained from sampled data for analysis and checking exponentiality which is not avilable in boxcar or

lock-in-amplifier system. Several other mathematical analysis can be done on this data.

3.3.3 Interpretation:

Besides DLTS technique another technique TATS(time analyzed transient spectroscopy) can also be used to determine trap parameters. In this, we take the constant capacitance voltage transient and plot it with $t_2/t_1=2$ and normalization of peak is done with simulated spectrum which gives emission time constant. This has advantage of constant temperature analysis.

Both of above techniques can be used to determine comparable results of desired trap level.

3.4 TSCAP Measurement:

Thermally stimulated capacitance(TSCAP) was originally used for insulator and later adapted to lower resistivity semiconductor when it was recognized that reverse biased scr is a region of high resistance.During the measurement the device is cooled, and traps are filled with majority carriers at zero bias[28]. Then device is reverse biased,heated at constant rate, and steady state capacitance is measured as a function of temperature. Capacitance steps observed as traps emit their carriers. T_m is the midpoint temperature of step and related to activation energy $\Delta E=E_c-E_T$ or E_T-E_v by

$\Delta E=kT\ln[(\gamma_n\sigma_nkT_m^4)/\beta(\Delta E+2kT_m)]$ trap concentration can be obtained by step height. This analysis gives approximate analysis of energy level and trap concentration compared to other mentioned techniques.

CHAPTER 4

RESULTS AND DISCUSSION

In this chapter, we first describe sample configuration used in this study and their preliminary characterization through I-V and C-V measurements. Then, we present results keeping trap characterization as the focus, and discuss these in the light of current understanding of radiation induced defects in silicon.

4.1 SAMPLE CONFIGURATION:

Silicon wafers used in this study had n-type epitaxial layer on n^+ substrate, commonly referred to as n/n^+ structure. The thickness of the epitaxial layer was 17μm and resistivity 15-20 Ω-cm. As-received samples had mirror finish on the top surface.

Schottky diodes were fabricated on the epitaxial layer by depositing gold film of 1000A thickness with e-beam vacuum evaporation. Ohmic contact at the back was made using thermal vacuum deposition of thick aluminum films.

Alpha particle irradiations were done using Van de Graaff facility at IIT Kanpur. Most of the irradiation were done using 1.3 MeV He^+ ions. Two sets of samples were prepared, one for which the irradiation angle was 65^0 and

the other at 63^0. The rationale behind the choice of energy and angle has been described earlier. All irradiations were performed at room temperature. The ion doses were between 10^{12}-10^{13} ions/cm^2. The minimum dose was limited by the resolution of current integrator. The maximum dose was chosen so as to keep the concentration of defects comparable to background shallow level dopants.

All measurements were done after fabricating the top metalization. Gold wire bonding to the top contact was done by using epoxy (compound A and B, Elteck Corp.). The epoxy was cured at 85^0C for 30 min in a laboratory oven. This is the only heat treatment that the sample received during the entire sample fabrication process.

The control sample for each set went through all the processing steps on the same wafer except for irradiation.

4.2. Preliminary Characterization:

Since our primary goal is to investigate deep level traps through capacitance spectroscopy methods, we need to ensure that the schottky diodes fabricated are of sufficiently good quality for the purpose. It should also be borne in mind that our effort is not to produce excellent schottky diodes in terms of I-V and C-V curves. The quality of the diode should be such that there is no excessive

current leakage making capacitance measurements invalid or difficult. Further, C-V characteristics should have the desired change of capacitance with voltage.

4.2.1 I-V Result And Analysis:

A typical set of I-V curve is shown in Fig.1 for damaged samples with two different irradiation doses. Note that reverse current clearly shows saturation, and the saturation level is less than 10 μA. Also note that the absolute values of the forward current is much smaller than expected, indicating presence of compensated high resistive damaged layers in the depletion layer. However the forward current has the desired exponential rise for low forward biased voltages.

4.2.2 C-V Measurements:

A set of typical $1/C^2$ vs V curves at room temperature is shown in Fig4.2. The control samples and irradiated samples have in most cases shown near identical slopes indicating that the irradiation with MeV α-particles with dose range 10^{12}-10^{13}ions/cm^2 does not change considerably the background concentration of active shallow dopants. The hump seen for control sample in fig 4.2 is artefactual and

gets removed on furnace annealing. Such features appeared in control sample, most probably due to variation in surface preparation prior to Schottky metal deposition. The use of better clean room procedures, than that available with us at present, can avoid this problem. However it does not affect our later trap specific investigations which are mainly spectroscopic in nature, and do not crucially depend on absolute values of device capacitance.

Further, the carrier concentration obtained from the slope of $1/C^2$ vs V curves is close to the background concentration of shallow-dopants(i.e. $2x10^{15}/cm^3$) consistent with resitivity of as-received epitaxial layers. Note that the absolute values of capacitance for all voltages is lower in the sample irradiated with higher dose implying larger depletion width for same reverse bias. This indicates that the damage caused compensation, most probably at the end of the ion range where the most of the energy of the ions get deposited causing severe damage. That would lead to larger width of depletion layer and hence lower capacitances. The gradual flattening of the $1/C^2$ vs V curve towards the low voltage side is also an indication of the fact that the depletion width gets limited to a minimum value. This is a further indication that a highly damaged and compensated layer has been formed. For these samples,we restrict our analysis only to those regions of C-V curve where the linearity prevails in $1/C^2$ vs V plot.

A typical set of $1/C^2$ vs V curves for a damaged sample is shown for various temperatures in Fig4.3. Note that with reduction in temperature the principal change observed is in the apparent built-in potential. This is understandable since the occupancy of the traps introduced by damage in the depletion layer control the effective built-in voltage. The gradual changes in the concentration of donors observed in these samples is consistent with expected carrier freeze-out and movement of the Fermi level of the sample with temperature.

4.3 Calculation of Ion Range and Damage Distribution

The ion and damage distribution calculations were performed using the 1992 version of the Transport of Ions in Matter (TRIM92) program developed by Zeigler et. al. [9]. The program takes , as input, the incident ion energy, the angle of incidence, the displacement energy E_d, the binding energy of the lattice atom to its site E_b and the thickness of the Si layer. The standard values of E_d = 13 eV and E_b= 1.5 eV have been used.

The program assumes an incident ion of atomic number Z_1 and energy E_1. It undergoes a collision with a target atom of atomic number Z_2 which acquires energy E_2 following collision. The condition to create target vacancies, phonons etc are enumerated below.

Condition	Consequence
1. $E_1 > E_2$, $E_2 > E_d$	A vacancy results
2. $E_1 > E_d$, $E_2 < E_d$	E_2 is released in the form of phonons.
3. $E_1 < E_d$, $E_2 > E_d$	Original atom remains at the site. The event is then called a replacement collision
4. $Z_1 \neq Z_2$	Z_1 becomes an antisite atom
5. $Z_1 = Z_2$	Z_2 merely reflecting Z_1 in the cascade & E_1 is released in form of phonons
6. $E_1 < E_d$, $E_2 < E_d$	Z_1 becomes interstitial & $E_1 + E_2$ is released in the form of phonons

The TRIM calculations were performed for two cases. One with the ion beam incident normal to the Si sample surface coated with a thin film of Au of 1000 A thickness and other with ion beam incident at an angle of 65^0 with respect to the surface normal. The ion trajectories with projection along X-axis, Y-axis, Z-axis are shown in Fig 4.4 and 4.5 for normal and oblique angle of incidence. The X-axis is normal to the surface. The He^+ ion distribution and the Si vacancy distributions are plotted for normal and oblique incidences in Figs.4.6 to 4.8. The He^+ ion distribution in case of normal incidence is located at 4.16 μm depth and has a straggle of 0.18μm. But in case of oblique angle

incidence, the ion range is 1.66μm with straggle of 0.34μm The vacancy distribution in both the cases is close to the ion distribution. The comparison of normal and oblique incidence justifies our choice of the oblique geometry to reduce the range of the damage distribution such that it appears in the region of interest.

4.4 DLTS Studies:

Fig 4.9 shows comparison of DLTS spectra of one set of samples consisting of control diode and samples irradiated with different doses. The peaks common to all the samples are labelled as E1 ,E2 and E3. Note that apart from these, there are other less well resolved peaks in the two damaged samples. We will consider detailed line shape of each peak separately in a later section.

All the observed peaks are majority carrier peaks. This is only to be expected since the experiments were carried out in Schottky barrier configuration, which is a majority carrier device. Hence we are only probing electron levels communicating with the conduction band. The presence of E2 in control sample indicates that it is a native defect which must have been introduced through either wafer processing or sample handling. However it does increase considerably in damaged samples. All other peaks make appearances only in irradiated samples, hence must be damage related. These

experiments were conducted for two sets of sample with similar results.

To determine the activation energies of the peaks, emission time constants as a function of temperature were determined by obtaining DLTS plots for different choices of ratewindow (i.e. gates t_1 and t_2 for sampling the transient).

A typical plot is shown Fig 4.10 for different rate windows for a dose of 1.12 x 10^{12} /cm^2. Then activation energy was obtained from Arrhenius plots for each of the major peaks by plotting $\log(e_n/T^2)$ vs 1000/T. Fig4.11 shows activation plot of peaks E1, E2 and E3 giving values of Ec-0.23 eV, Ec-0.41 eV and Ec-0.28 eV respectively. These plots are signature of specific traps and can conveniently be used for assigning origin of these defect levels. The slope yields activation energy and its y-intercept the capture cross section. The sample irradiated with high dose (2.8 x 10^{13} /cm^2) also yielded similar results. Arrhenius plot for peak E3 in high dose sample in Fig. 4.12.

The peaks corresponding to Ec-0.41 eV and Ec-0.23 eV have been found in almost all irradiation work [2, 6, 17] in n-type silicon. Svensson et al [11] have recently studied these defects in n-silicon after irradiating with electrons, and ions of He, O and Br. These peaks have been

assigned to different charge states of divacancies through correlation of EPR, IR and ENDOR alongwith electrical characterization using DLTS. Though there have been contraversies regarding exact properties and nature of these defects, this identification of origin seems to be beyond doubt. The Ec-0.23 eV peak is attributed to $V_2(=/-)$ and Ec-0.41 eV peak to $V_2(-/0)$, where V_2 stands for divacancy and signs in braces indicates transition from initial charge state occupied with an electron to a final charge state after emission of an electron to the conduction band. The capture cross-section obtained for these two defect levels are $5.7*10^{-15}cm^2$ for Ec-0.23eV and $3.3*10^{-15}cm^2$ for Ec-0.41eV respectively. These are in good agreement with the values obtained by other authors[2, 11, 17].

The third major high temperature peak E3 has been observed for the first time in α-irradiation material. Since in this work we have taken care to keep the buried layers close to the surface (i.e. within a few microns) and the doses employed are high, we expect to see other damage related defects within the depletion layer. The peak E3 seems to be one such damage related peak in large concentrations as can be seen from DLTS spectra of Fig4.9. For many choices of rate windows, it appears close to the Ec-0.41eV level and hence spectroscopic reconstruction were done to isolate its peak. This is described in more detail in a later section on lineshape

analysis. It is interesting to note that the concentration of this level goes down drastically as the rate window is increased or, in other words, as the peak appears at lower temperatures. This feature will be discussed later. The Arrhenius plot for this peak is also shown in Fig 4.11. Since the peak height goes down severely for low temperature peaks, only small number of points have been used in the Arrhenius plot. However to make sure that there are no significant mistake in obtaining the energy and capture cross section, detailed simulation of these peaks were done to obtain the values Ec-0.286eV and $\sigma_n \simeq 1.9*10^{-19} cm^2$.

Though the energy of the peak E3 is smaller than E2 (i.e. Ec-0.41ev) peak, its DLTS peak appears at a higher temperature. This is due to the fact that capture cross-section of the defect level is very small, almost four orders of magnitude smaller than E1 and E2. Therefore the appearance of the peaks in temperature is non-sequential in terms of energy. The fact that the activation energy is small for this peak can be seen from the smaller movement of the peak with similar changes in rate-windows for other peaks.

At the moment we can only attribute the peak E3 to damage without assigning any definitive origin. Such small capture cross-section does indeed imply a negatively charged unoccupied state with repulsive character for an electron. Hence this defect level may not act as an effective trapping

centre. However, it certainly contributes to the increase in depletion width even when unoccupied, since it is negatively charged and hence counters the presence of positively charged background shallow donors. From survey of DLTS, the basic parameters of the three major peaks are summarized in table 4.1.

4.5 TATS of (Ec-0.41eV) Peak:

As pointed out in chapter 3, the spectroscopy of defects is best done by Time analyzed Transient spectroscopy (TATS) to take into account detailed lineshape. In order to validate our DLTS analysis, we chose to carry out TATS analysis of the most well behaved peak of the three. The concentration of Ec-0.41eV is of the order of the damage related peak as seen from DLTS spectra. Hence it was enough to check TATS results for this peak. The TATS spectra for Ec-0.41eV peak for different choices of γ is shown in Fig4.13(a). The corresponding Arrhenius plot is shown in Fig4.13(b). It agrees very well with the results obtained from DLTS spectra. Fig. 4.13(a) also shows the simulated TATS peaks which matches well with the experimental lineshape. This confirms that DLTS is sufficient for characterizing defects in these materials. Hence we choose to do line shape analysis using DLTS only.

4.6 TSCAP Studies:

Thermally Stimulated Capacitance (TSCAP) is another

useful method of characterizing these levels. It is specially advantageous in ascertaining total concentration, since filling is done for a long time at a lower temperature and the step height in capacitance as a function of temperature is indicative of total concentration of trap. Moreover this being a quasi-equilibrium method, the signal noise to ratio is very high. Fig 4.14 shows TSCAP spectra for both low dose and high dose samples. The corresponding differentiated signals are shown in Fig.4.15 in which steps in TSCAP appear as peaks.

The steps observed at around 160^{0}K in both the spectra correspond to Ec-0.41eV level of the divacancy. The TSCAP step corresponding to Ec-0.23eV level is not expected within this range of temperatures. The peak corresponding to Ec-0.28eV i.e. the damage related level is not seen in these spectra. This is understandable since it is already clear from DLTS results that the concentration of occupied states decreases rather drastically even by lowering the peak temperature by 15 ^{0}K. In case of TSCAP, filling pulse is provided near 100^{0}K. Hence it is expected that the damage related peak do not get filled at such low temperatures. This explains their absence in TSCAP spectra. The concentration values obtained from simple use of step height in TSCAP is $\simeq 7.95*10^{13}/cm^{3}$, assuming that all traps accessible by filling pulse do get occupied.

Energy determination using TSCAP was not carried out since widely different heating rates are needed for the purpose. At present we do not have facility for temperature programming of the sample to obtain large linear heating rates. However energy values were estimated from the occurrence of the step position. The estimated values agree with the identification that it is the $V_2(-/0)$ level corresponding to point defects. It can be said that the concentration is not so high as to invalidate standard DLTS analysis of lineshape.

4.7 LINESHAPE ANALYSIS OF DLTS SPECTRA:

The high concentration levels of the Ec-0.41 and Ec-0.28eV raises the question whether DLTS lineshape corresponds to exponential transients. Exponential transients are expected only when the defect concentration is small as compared to the background doping. Further, since relatively high doses have been used to create defects, it is possible that the defect levels are broadaned in energy giving rise to distribution in density of states in the band gap. Hence it is necessary to ascertain existence of non-exponentiality, if any, of transients.

Fig 4.16 shows an experimental DLTS spectrum for low dose sample. Note that the peak corresponding to Ec-0.41eV looks broadened. A simulated normalized peak using the

values of energy 0.41eV and its corresponding capture cross section is shown in the figure. It is difficult to say from this spectrum alone whether there is a continuous energy distribution or overlapping of multiple single energy defects to produce this effect. However if we look at the sample's DLTS spectrum at a different rate window such that the peak corresponding to Ec-0.41eV moves to lower temperatures, the peak becomes perfectly exponential. Hence this proves that the Ec-0.41eV is not broadened by itself as has already been confirmed by TATS analysis as well. The damaged layer being probed by DLTS has only electrical point defects.

Fig 4.18 shows the peak corresponding to Ec-0.41eV level for the high dose sample with 2 ms ratewindow. Surprisingly, in contrast to the results on low dose sample, even at this ratewindow the DLTS lineshape corresponds to perfectly exponential signal. Note the close matching between the simulated and exponential line shapes. What this means is that electrically active defects other than divacancy have changed their energy positions in high dose samples. The spectrum in Fig4.18 clearly shows that other unidentified damage related peaks now occur at higher temperature.

These observations indicate that though stable native defects produced by irradiation appear at the same energy

position in the sample of different doses, the energy spectrum of damage related levels is sensitive to the amount of damage created. In this sense, the doses used are high i.e. the dose of irradiation is able to modify the electronic states of defects. The dose is not sufficient to produce amorphization but may be enough to introduce strain effects at the high damage region. The defects being probed are at the end-of-ion range and are sensitive to the stress in their environment. It is known that heavier ions are capable of creating highly disordered region locally.

Svensson et al [11] have used projectiles of different masses (electron, proton, He, O, Br) to compare lineshapes of E_c-0.41eV level. They have observed progressive peak broadening with increase in mass of the projectile. This is attributed to large locally strained enviornment for the point defects in case of heavier ions. Our results show that α-particles do not produce broadening in energy on incresisng the dose. Hence He^+ can be used to create more isolated point defects without causing local disorder around them. However He^+ does introduce other types of point defects on high doses, for example, the E_c-0.28eV level as observed by us. The dose of $10^{13}/cm^2$ is not high enough for creating damages which change the point defct nature of generated defects.

4.8 Defect Profile:

We have carried out depth profiling of E_c-0.41eV

vacancy related level by repeating DLTS scans for different choices of depletion width. Fig 4.19(a) shows the experimental results. The depth calculation on the x-axis of the figure is done from capacitance value of the Schottky diode. Fig 4.19(b) shows the vacancy distribution predicted from TRIM92 simulations. For the energy and angle of incidence used, simulations predict that the ion range is approximately 1.7μm. However, note that experimentally peak value is obtained at 2.8μm. We argue that the depth calculated from the depletion width is only an apparent depth. The damage and defect caused by ion bombardment decrease the contribution of backgroud shallow levels to change in the depletion layer either by deactivating shallow dopants, or by compensating charge through creation of traps levels. For example, the trap level at E_c-0.28eV observed in our experiments is supposed to be negatively charged, even when unoccupied, and occurs in fairly large concentrations. The accumulation of such negative charges in the depletion layer would cause increase in depletion width, as has been observed . Hence, the defects studied do lie inside the depletion region.

Fig4.20 shows a simple schematic of band bending of an n-type Schotttky barrier diode having a trap at a certain distance from the surface within the depletion layer. At a certain bias of device, the Fermi level E_F would cross the trap level E_T. Only those traps falling below E_F would get

occupied even if they are within the depletion layer. As shown in (b) part of the figure. Now, if reverse bias is increased so as to push the depletion width wider, previously occupied levels would get exposed above the Fermi level E_F and would emit carriers into band. Thus, though the depletion width edge is deeper in the sample, traps emit from a distance closer to the surface. We propose this as a model to explain the difference observed in location of the peak from TRIM92 predictions. This would mean that the amount of reduction in positive charges corresponds to a change of 1.1 μm in depletion width carrying $1.0*10^{12}cm^{-3}$ dopants.

Note that except for this discrepency, we have been able to obtain the profile of the defect at the peak of concentrations. This indicates that we have been able to profile the defects at the ion range itself. This has been ensured by the fact that the damaged layer is created inside the depletion layer.

Fig.4.21 shows normalized depth profiles both predicted (a) and observed (b). Note that the full width at half maximum (FWHM) of the two normalized peaks are almost identical.

The fact that there is no appreciable broadning of depth profile from that predicted from simulations is in good agreement with the model of Paletshofer and Reisinger[10]. According to their model, electric field

enhanced diffusion normally leads to such broadening. However, no such broadening is expected if ions are irrdiated directly into the space-charge layer of a Schottky barrier diode.

The level of peak concentration observed by us is the highest among all reported studies with He^{+} MeV ions. Yet, note that the standard DLTS analysis holds since the background doping is also high ($1*10^{15}cm^{-3}$).

In the next chapter, we summarize and list the major conclusions of the study. We also indicate possible direction of extending this work.

CHAPTER 5

SUMMARY AND CONCLUSION

The study of damage and electrically active traps induced by He^+ ions in semiconductors is important from both fundamental and application point of view.In order to be able to study the effect of high energy He^+ ions in Si, irradiation were performed at an angle so that the range of the particle is well within the limits that can be probed by standard capacitance spectroscopic methods.The damage profile was studied by TRIM92 simulation. the effect of irradiation were studied using trap spectroscopic methods such as TSCAP, DLTS, TATS. Preliminary sample characterization using I-V and CV techniques were also carried out. This study is limited to n-type Si and majority carrier traps only.

The findings of the study can be summarized as follows:

(i) Three major peaks are detected by DLTS in an n-type silicon Schottky barrier irradiated with alpha particles at an angle. The peaks corresponding to energies 0.23eV and 0.41eV are identified to be due to the two different change states of divacancy V_2 in Silicon.

(ii) A majority carrier high temperature peak of large concentration has been observed to occur for the first time

in α-irradiated samples. Though the energy of this peak is relatively low at Ec-0.28eV, it appears at higher temperature due to its low electron capture cross-section. On the basis of capture cross-section this level appears be a repulsive centres for electrons.

(iii) The concentration of the $V_2(=/-)$ peak at Ec-0.21eV is found to be smaller than the corresponding $V_2(-/0)$ peak at Ec-0.41eV peak. This is most probable due to larger strain caused by high dose implants.

(iv) There are other unidentified traps whose occurance was dependent on the dose.

(v) The traps identified were all pcint defects and did not show any broadening in energy level though doses(10^{12}-10^{13}/cm^2) were used to induce there. This was concluded from careful analysis of the lineshapes.

(vi) The defct profile of divacancy level is experimentlly obtained from vriable filling pulse DLTS measurements, and was compared with vacancy distribution obtained from TRIM92. The depth obtained from space charge widths turn out to be apparant depths and a model is proposed to explain difference.

(vii) The FWHM of depth profile of vacancies predicted by simulation is in good agreement with the profile obtained for divacancy level V_2.

In summary, this work demonstrates several advantages of using oblique incidence geometry in inducing damage and deep level defects by MeV α-particles in n-type silicon. The advantages ; accured from the fact that range of ions can be

limited without specifying use of high energy and high dose to produce large number of defects.

The work has inter alia fulfilled the need of developing a clean method to creat controlled amount of well-characterized point defects for purpose of future in-house calibration in semiconductor laboratery it IIT Kanpur.

This work opens up many possibilites for future work. One obvious extension would be to carry out similar studies in p-type silicon to characterize hole traps. These can be done for wider ranges of ion dose. Direct methods measurements of capture cross-section using variable pulse DLTS would be necessary for more detailed understanding of the defects, specially for un identified peaks in DLTS. Annealing behavior of the individual point defects would give hints regarding their origin. This can mature into a tecnological tool to enable control of carrier lifetime at pre-calculated depths by introducing required number of defects.

BIBLIOGRAPHY

1.Radiation Effects in Semiconductors (Inst. Phys. Cond. Series)

2.Troxell J.R.,Solid State Electronics,vol 26,p539,(1983)

3.Borland J. and Koelieh R.,Solid State Technology,(1995)

4.Golanski A.,Appl. Surf. Sc. vol.43,p200,(1989)

5.Fahrunoc W.R. and Klausmann,Solid State Phenomena,vol.142,p85,(1988)

6.Kimerling L. C.,IEEE Trans.on Nucl.Sci.,vol.NS-23, no-6,(1976)

7.Timothy C.M.,IEEE Trans.on Electron Devices, vol.ED-26 no 1,(1979)

8.Takeuchi K.,IEEE Trans. on Electron Devices,vol.37 no 3,(1990)

9.Ziegler J.F.,in."Ion implantition science and technology",ed Ziegler J.F. p51.

10.Palmetshoter L.etal. J.Appl.Phys.72(6) p2167,.(1992)

11.Svensson B.G. etal.Physical Review B vol.43(3) p2292,(1991)

12.Schroder D.K.in "Semiconductor material and device characterization",pub.John Wiley & Sons

13.Lannoo M.in "Point Defects in Semiconductors:Theoretical",(Springer Verlag,NY),(1962)

14.Bourgoin J.C.and Lannoo " Point Defects in Semiconductors:Experimental",(Springer Verlag NY),(1962)

15.Jaros M.in "Deep Levels in Semiconductors ,(Adam

16.Lang D.V., J. Appl.Phys.,vol.45,no.7,(1974)

17.Indusekhar H,.Phys.Stats.Sol.(a) vol.93,p645,(1986)

18.Watkins G.D. and Corbett J.W.,Phys.Rev. vol.138,A543(1965)

19.Cheng L.J.etal ,Phys. Rev.,vol 152,p671,(1966)

20.Berman L.S.,Soviet Phys.- Semicond.,vol.15,p665,(1981)

21.Zafer N. and Iqbal M.Z.,J.Appl.Phys., vol.68 no 2,(1990)

22.Ramakrishnan K. M.Tech.Thesis, IIT Kanpur (1994).

23.George J.in " Preparation of Thin Films",Marcel Dekker, Inc.NY.

24.Feldman L.G. and Mayer J.M. in "Fundamental of Surface and Thin Film Analysis" North-Holland NY.

25.Banerjee N.,Ph.D.Thesis IIT Kanpur India (1993)

26.Sze S.M.,in "Physics of Semiconductor Devices" 2e,Wiley Eastern Limited.

27.Blood P.,Semicond.Sci.Technol. vol.1,p7,(1986)

28.Schroder D.K. in "Semiconductor Material And Device Characterization",publ.John Wiley & Sons,Inc.

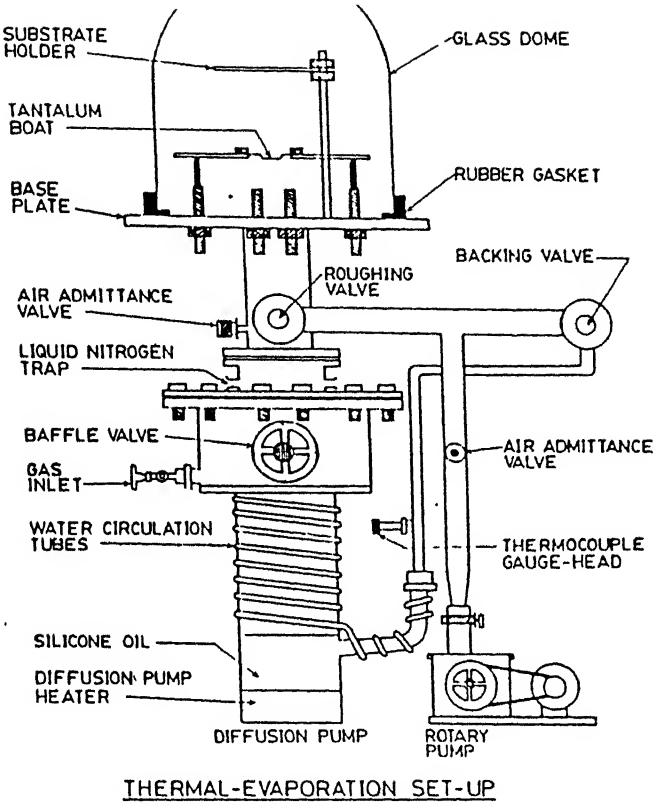

Fig. 2.1(a) Schematic Thermal deposition unit.

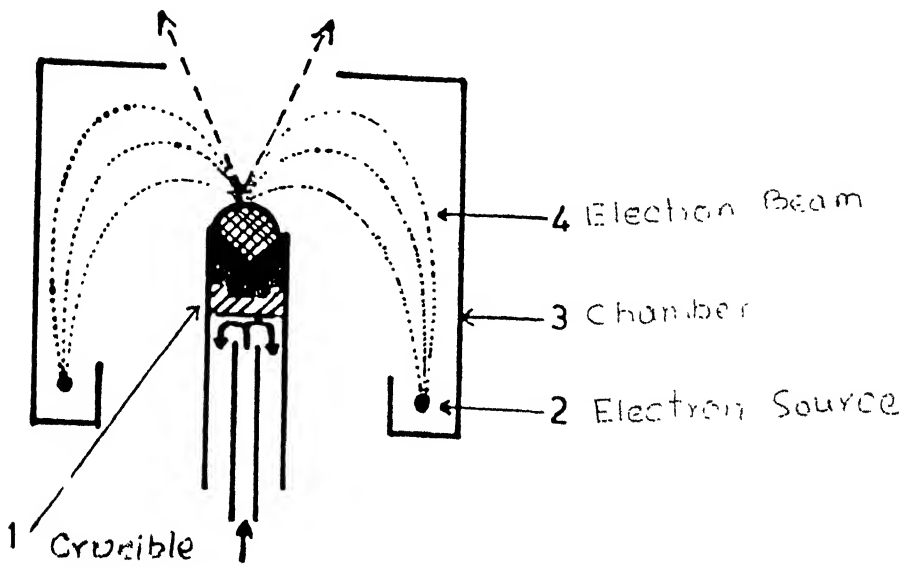

Fig. 2.1(b) Schematic Electron beam deposition unit.

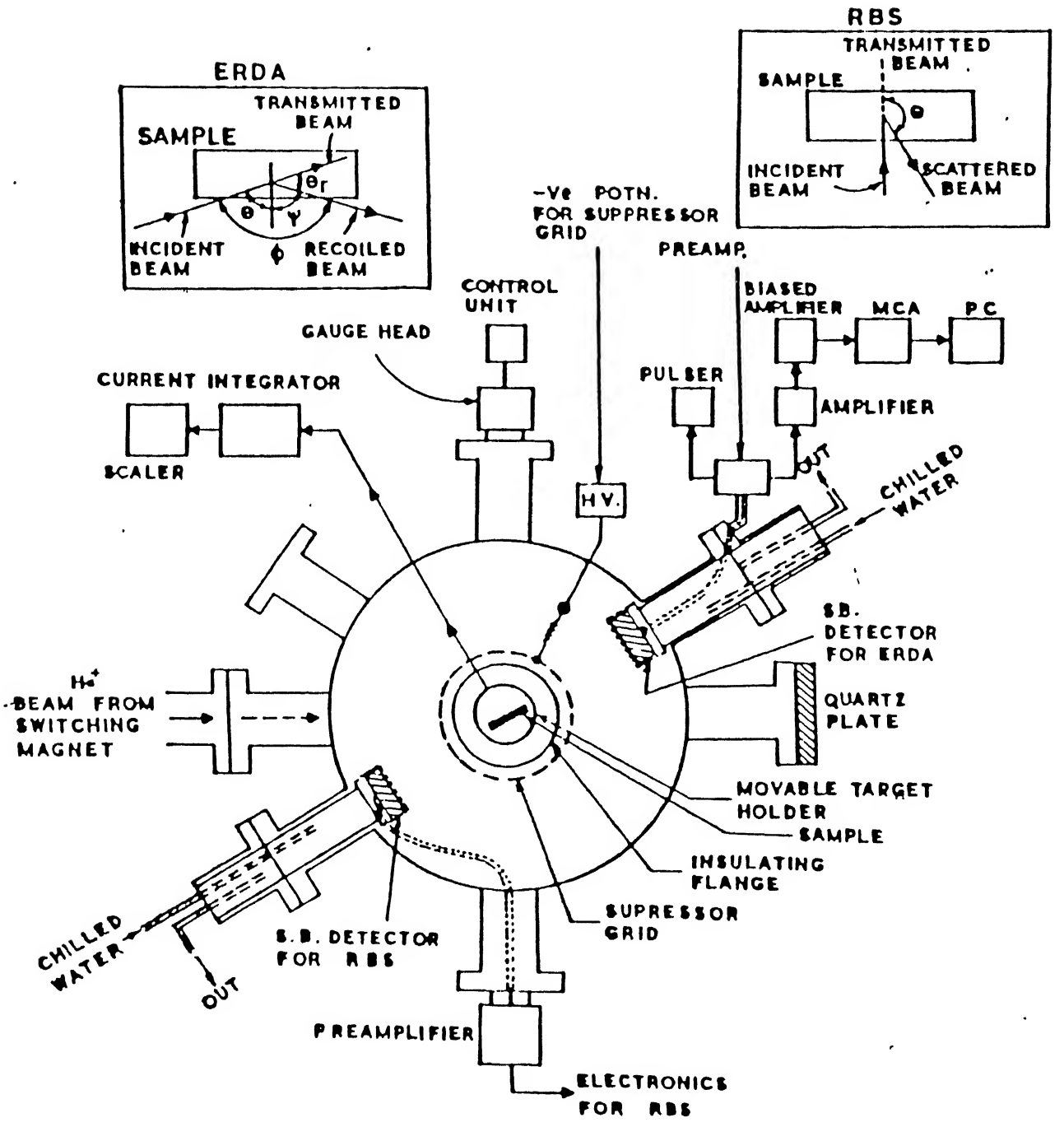

Fig. 2.2. BLOCK DIAGRAM OF THE CHAMBER AND ASSOCIATED ELECTRONICS FOR RBS AND ERDA MEASUREMENTS.

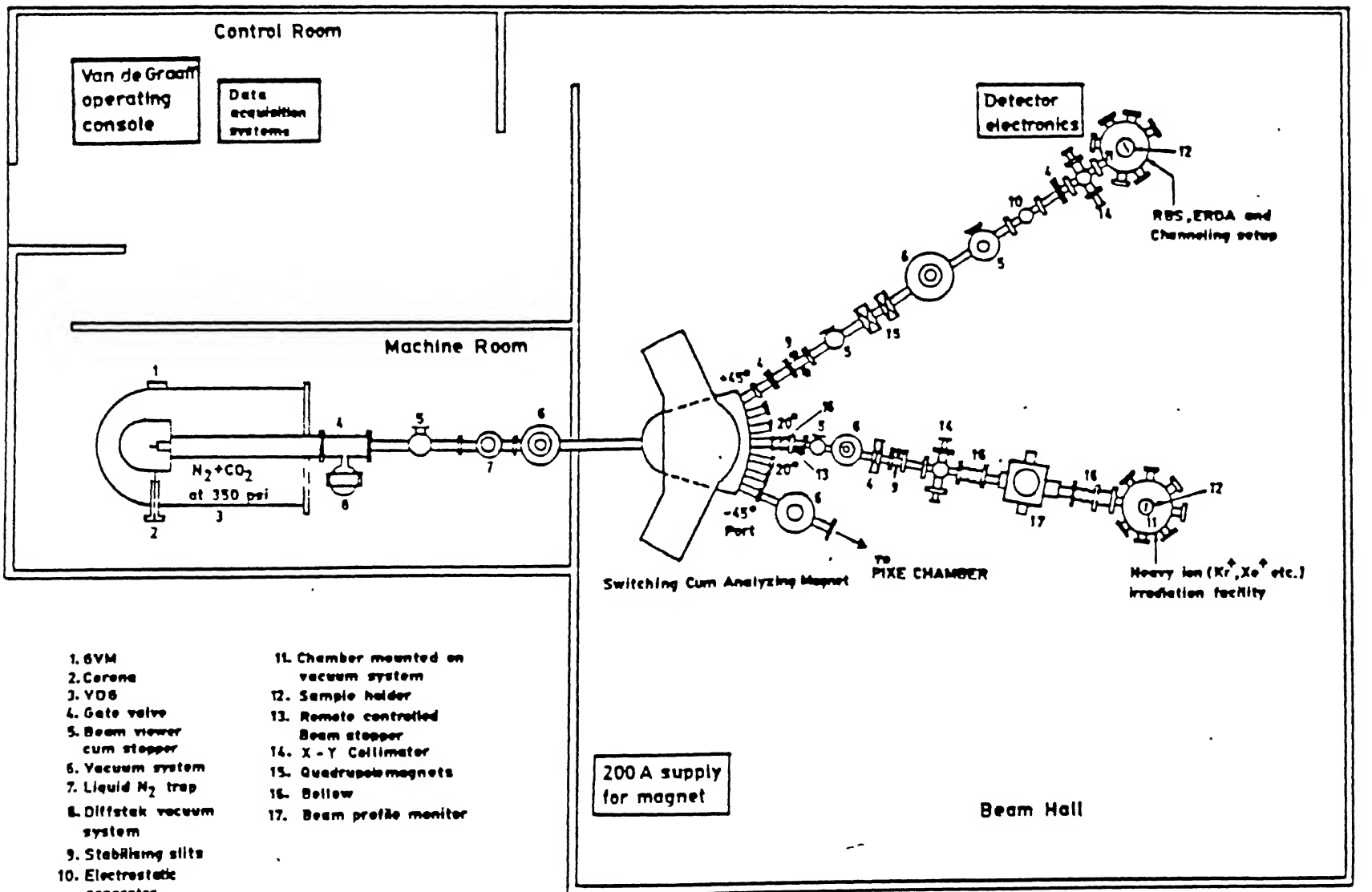

Fig. 2.3 LAYOUT OF ACCELERATOR SET UP.

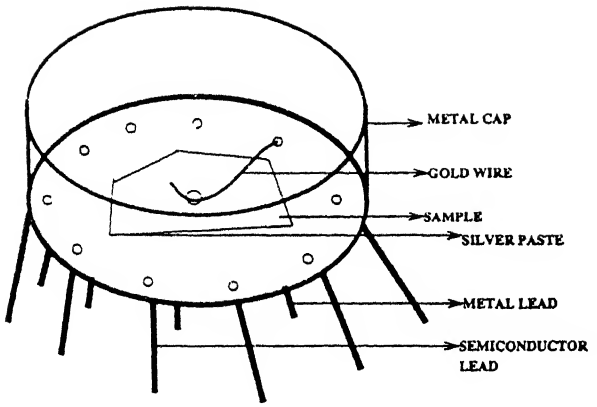

g. 3.1(a) Structure of Mounted Schottky Diode

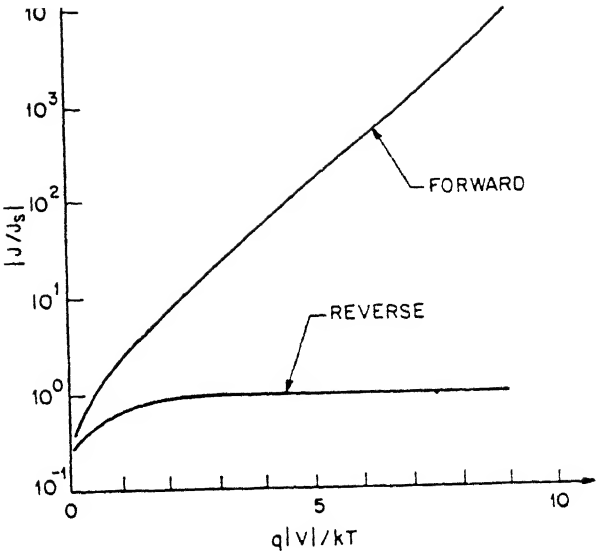

Fig. 3.1(b) Ideal I-V curve.

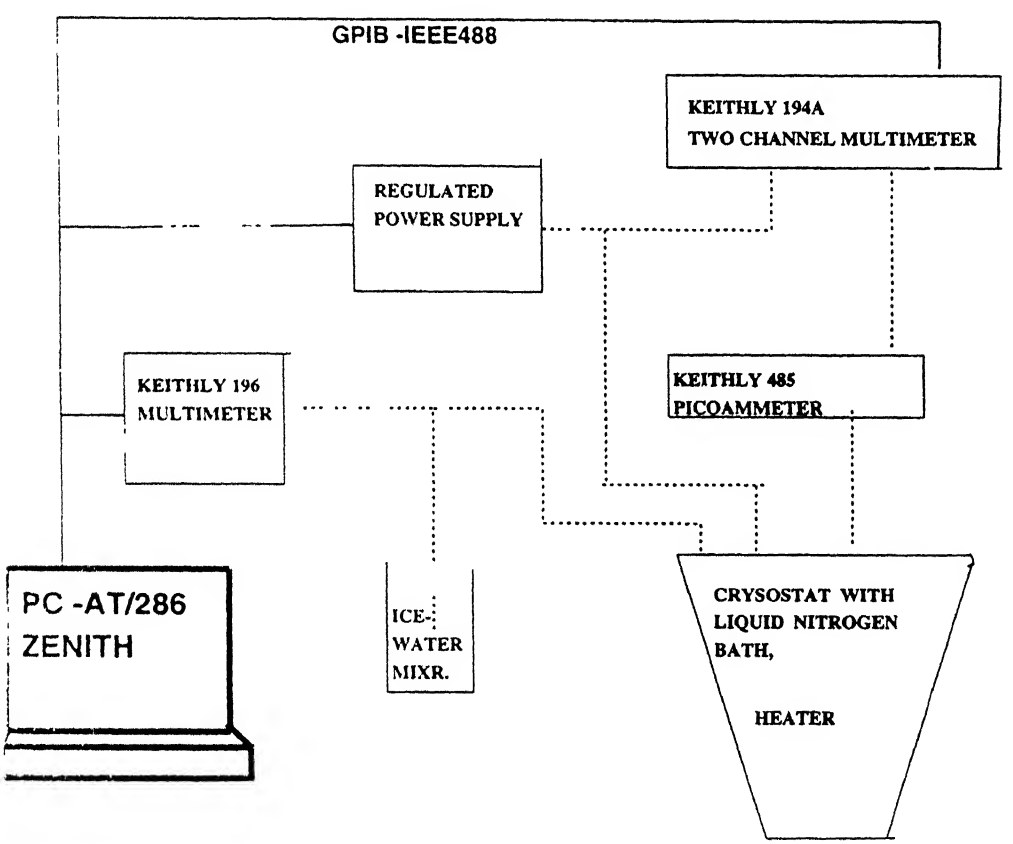

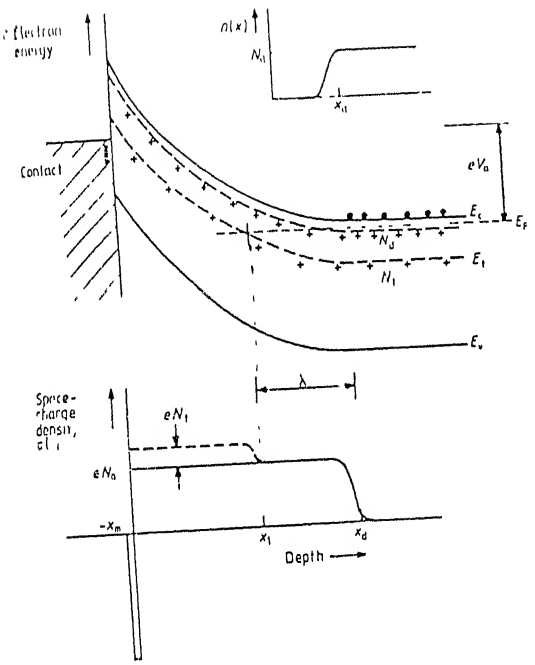

Fig. 3.2(a) Band bending diagram in reverse bias condition.

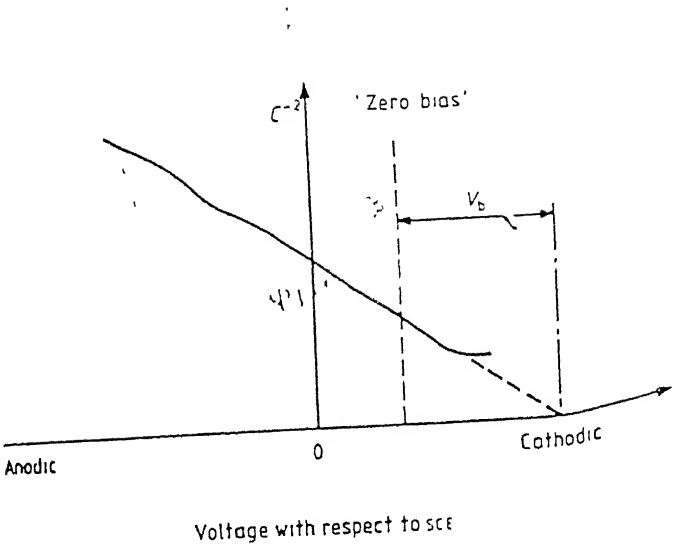

Fig. 3.2(b) Ideal $1/C^2$ vs V curve.

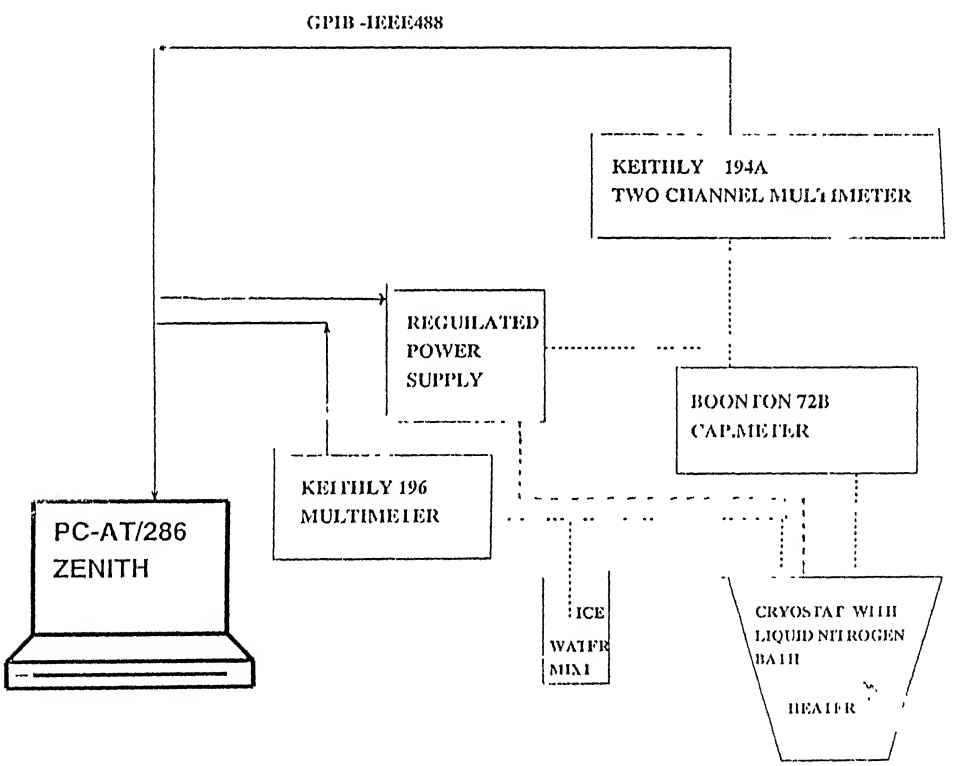

Fig. 3.2(c) Set up for capacitance-voltage measurement.

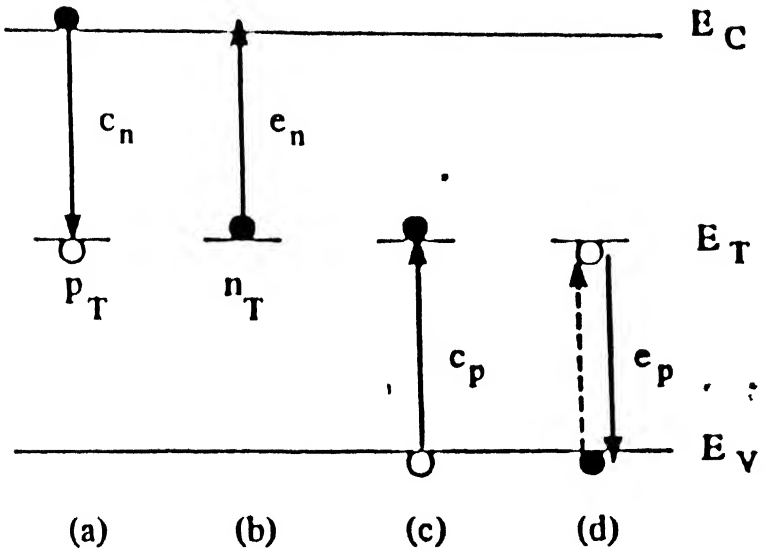

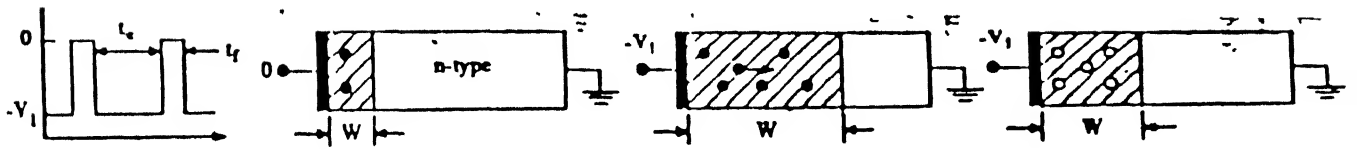

Fig. 3.3(a) Fundamental process of Generation-Recombination centres.

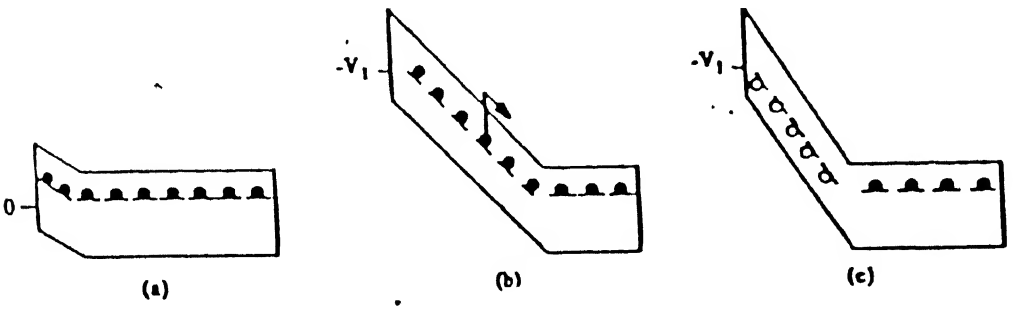

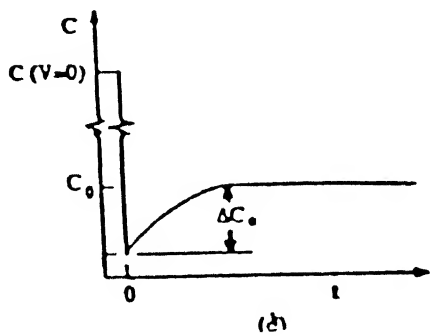

Fig 3.3(b) Capacitance vs time diagram

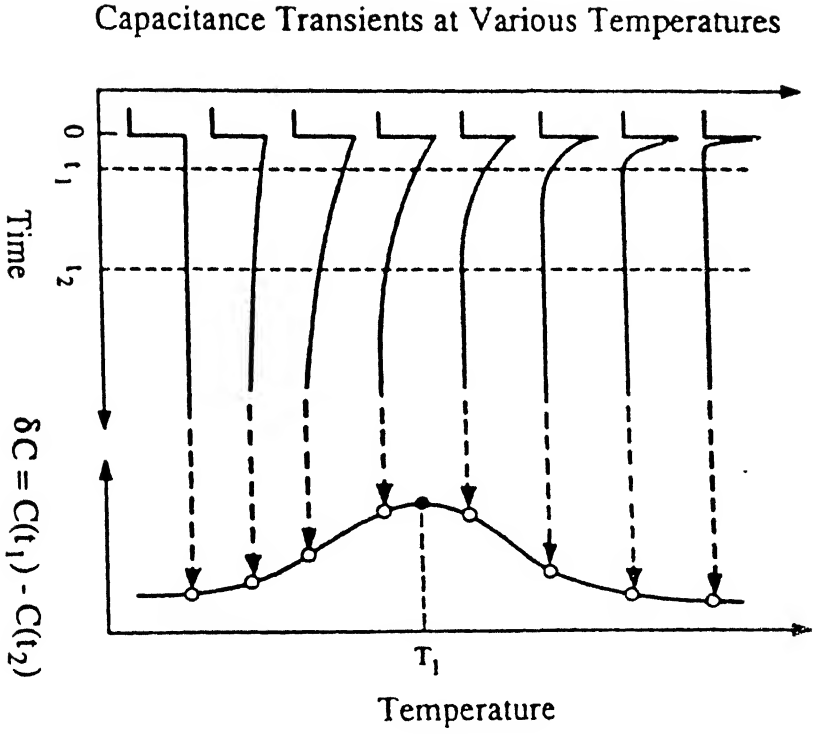

Fig. 3.3(c) Transient emission rate and Construction of Boxcar signal

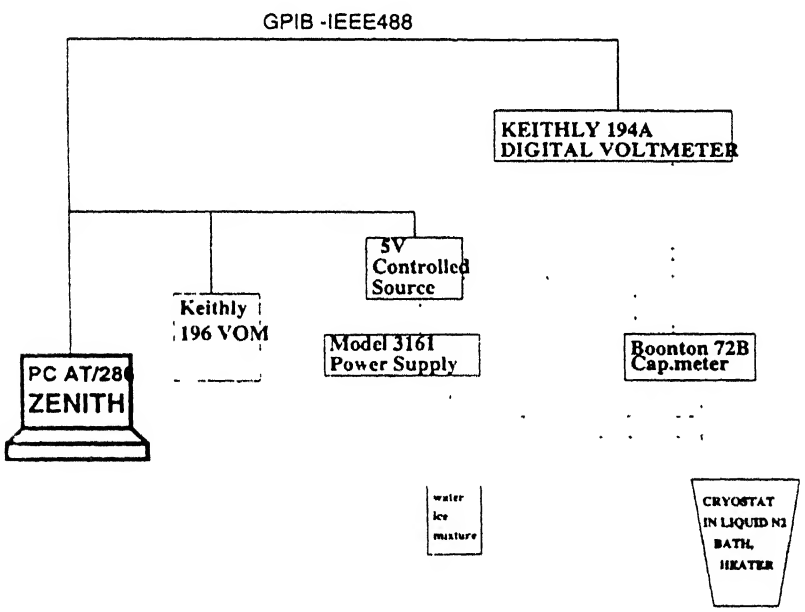

Fig. 3.3(d) Set up for transient measurement.

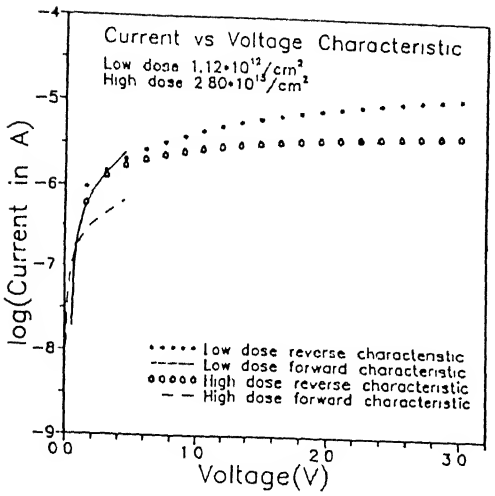

Fig. 4.1 Current vs Voltage Characteristics of damaged sample.

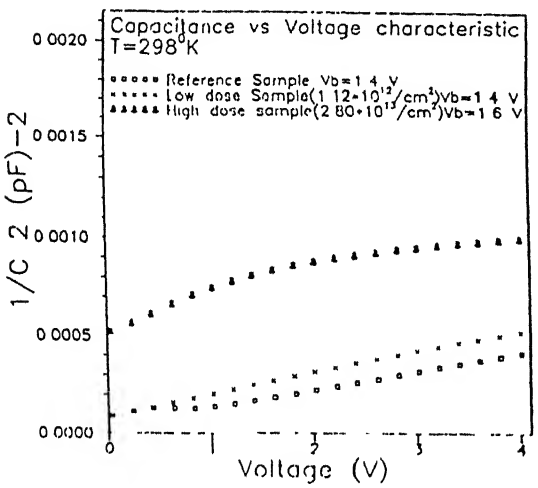

Fig. 4.2 Capacitance vs Voltage Characteristics of damaged sample.

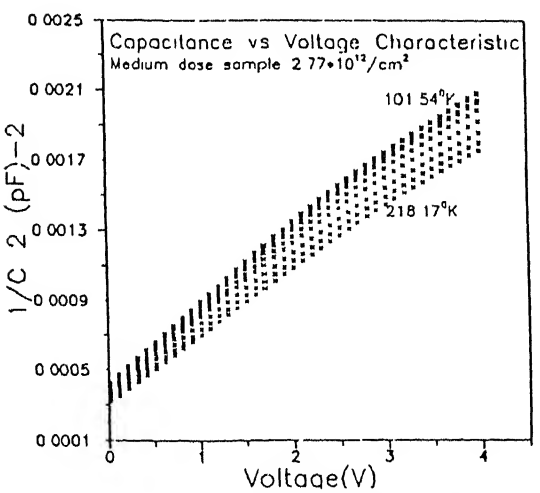

Fig. 4.3 Capacitance vs Voltage Characteristic for medium dose sample at various temperatures.

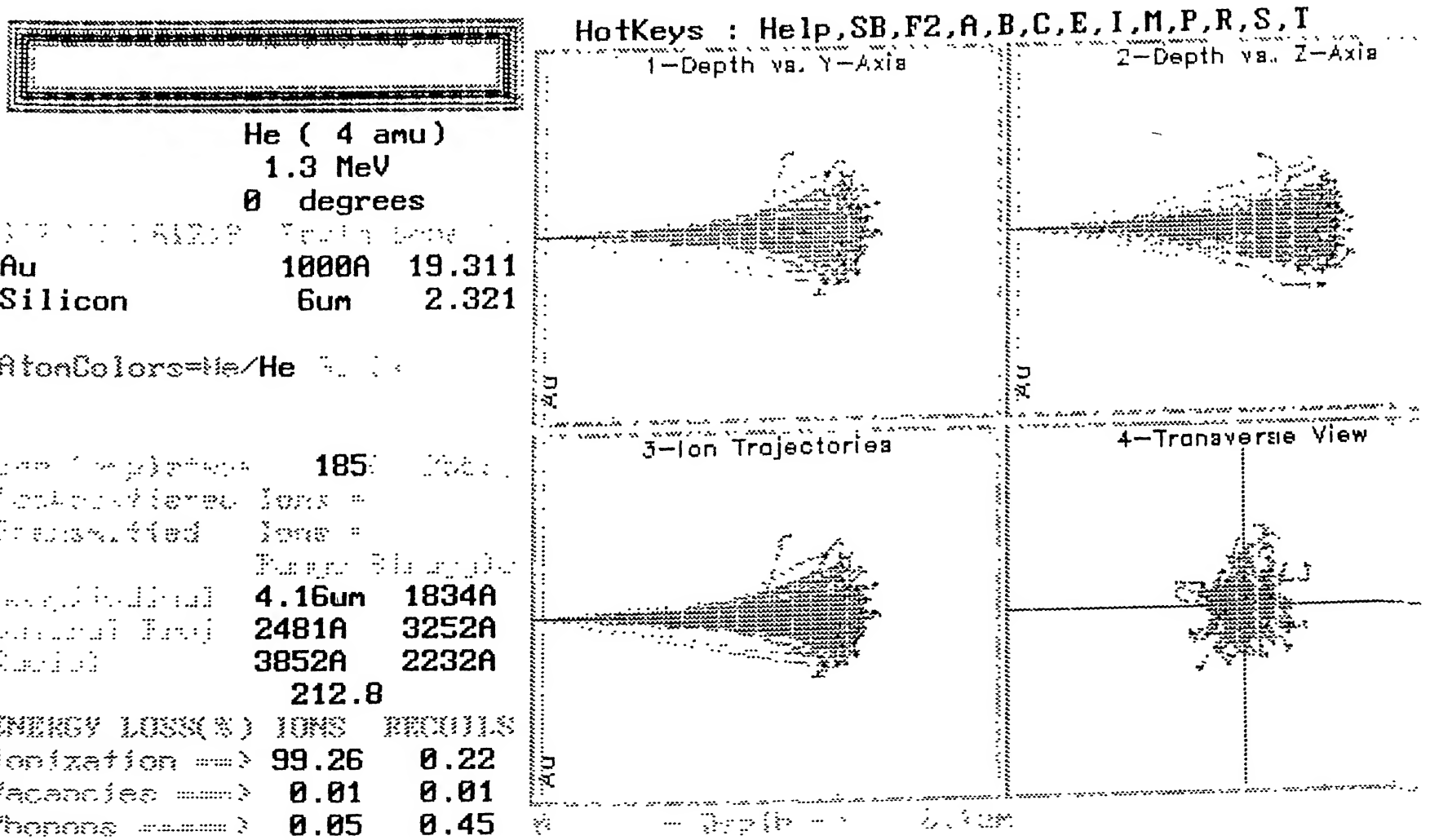

Fig. 4.4 TRIM92 simulation for He^{+} Ions(1.3MeV,0^{o}) showing Ion trajectory and displacement in Silicon.

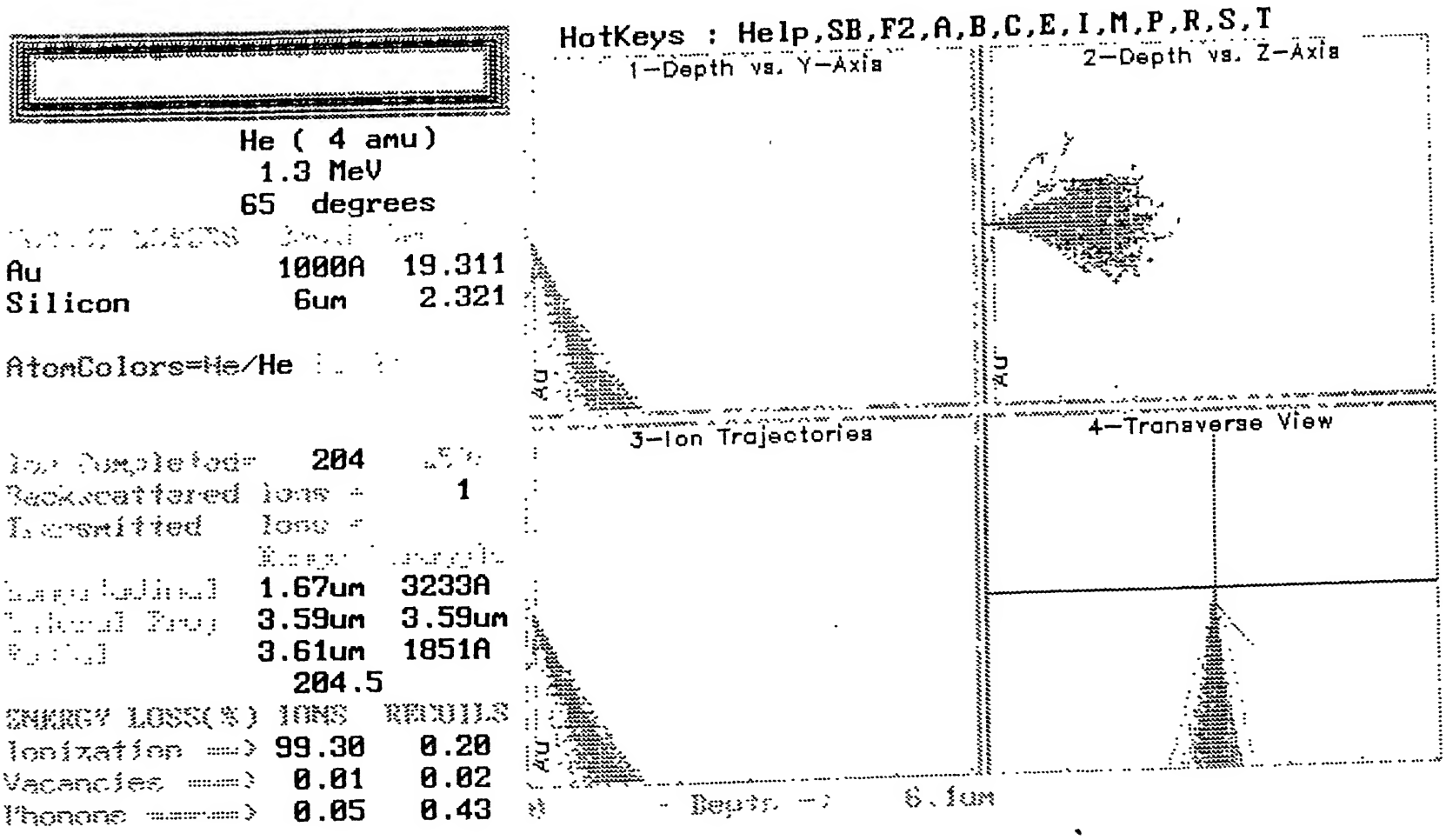

Fig. 4.5 TRIM92 simulation for He^+ Ions(1.3MeV, 65^0) showing Ion trajectory and displacement in Silicon.

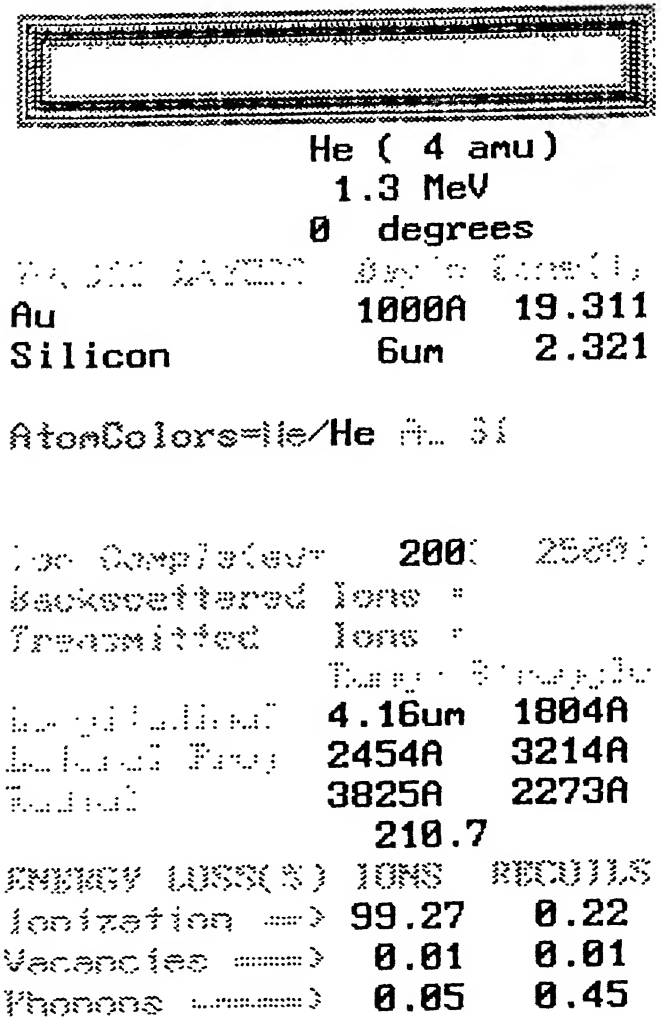

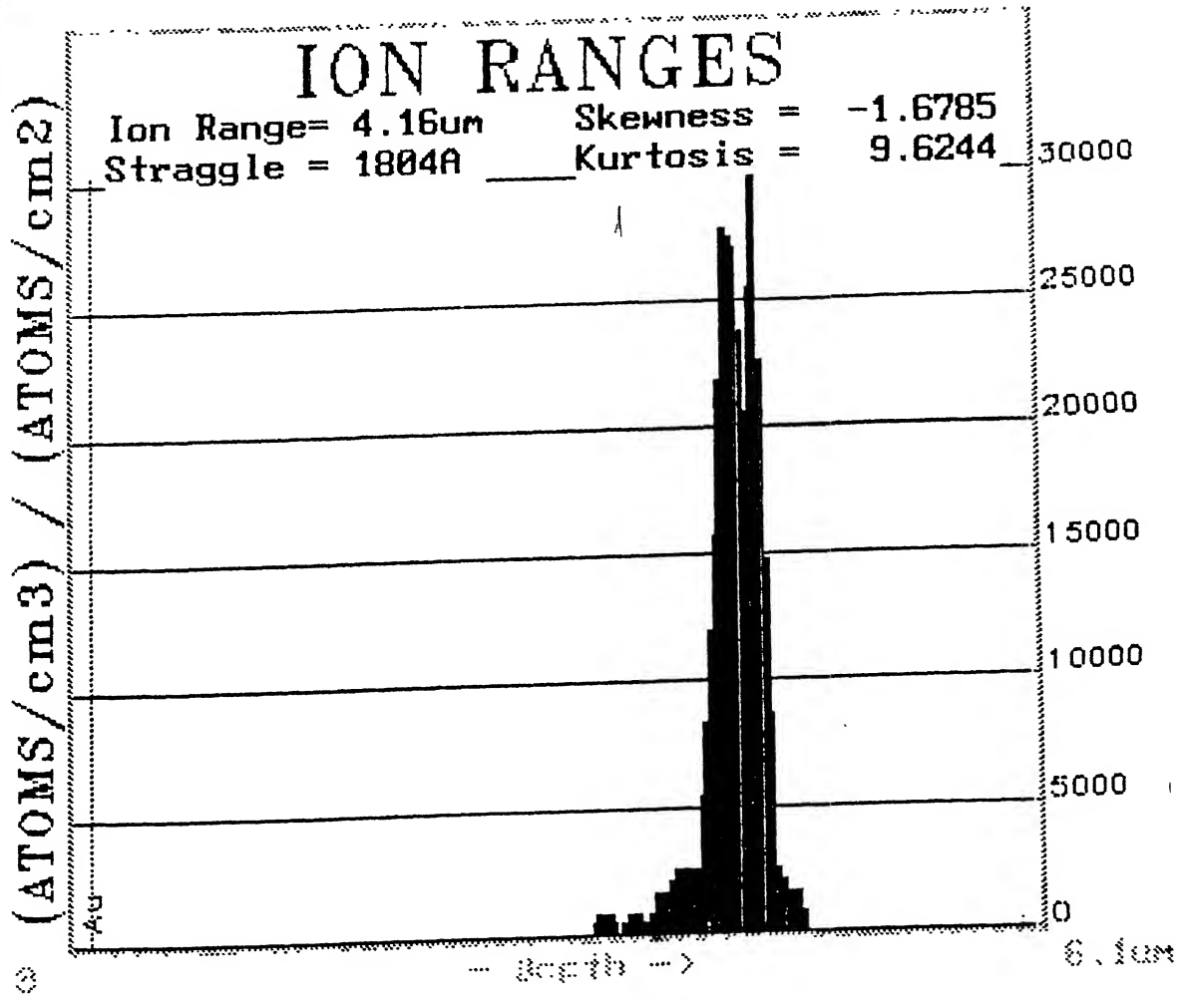

Fig. 4.6(a) He^{+} Ions(1.3MeV,0^{0}) Profile in Silicon

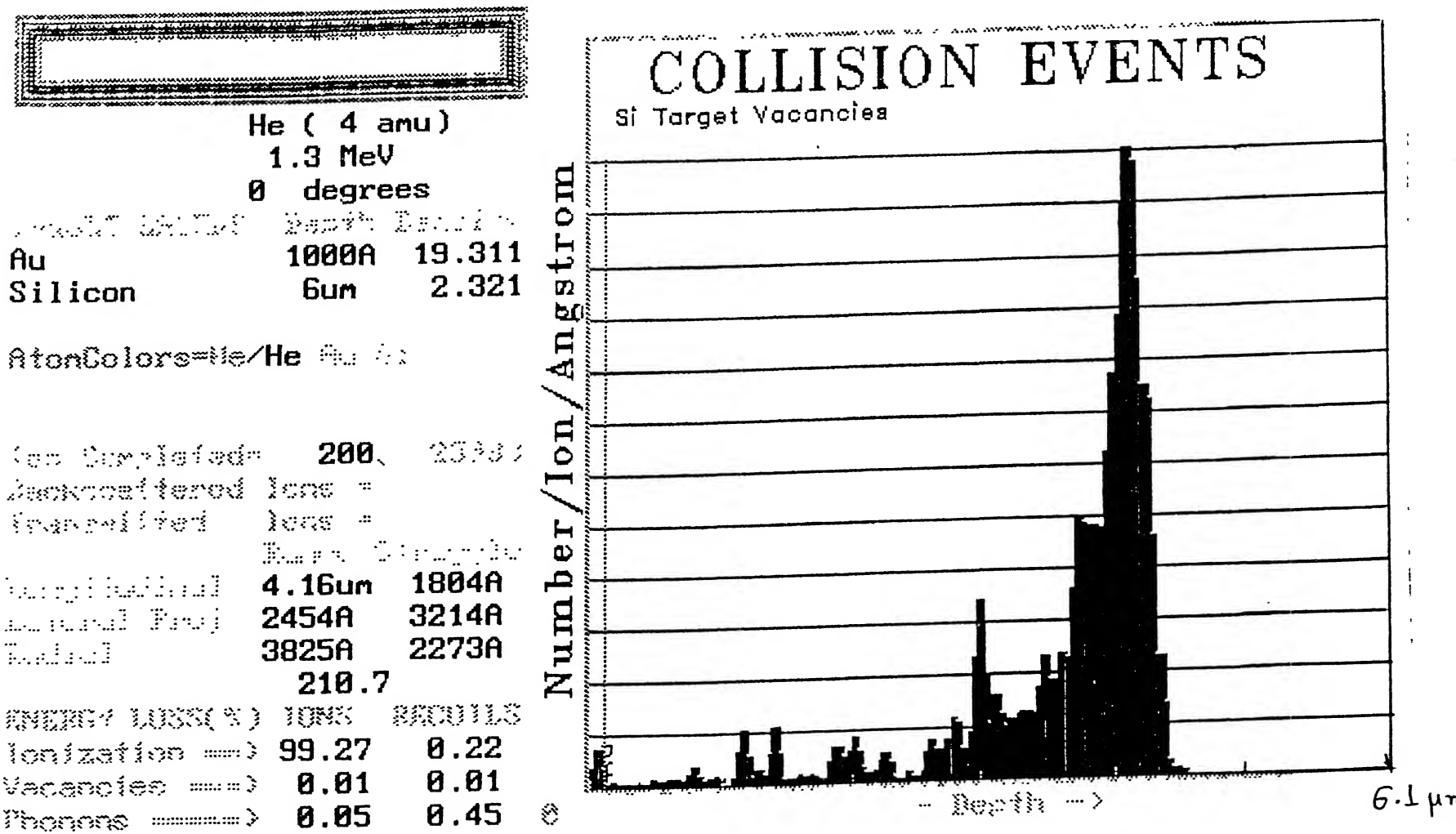

Fig.4.7 Vacancy Profile in Silicon induced by He^+ Ions(1.3MeV, 0^0)

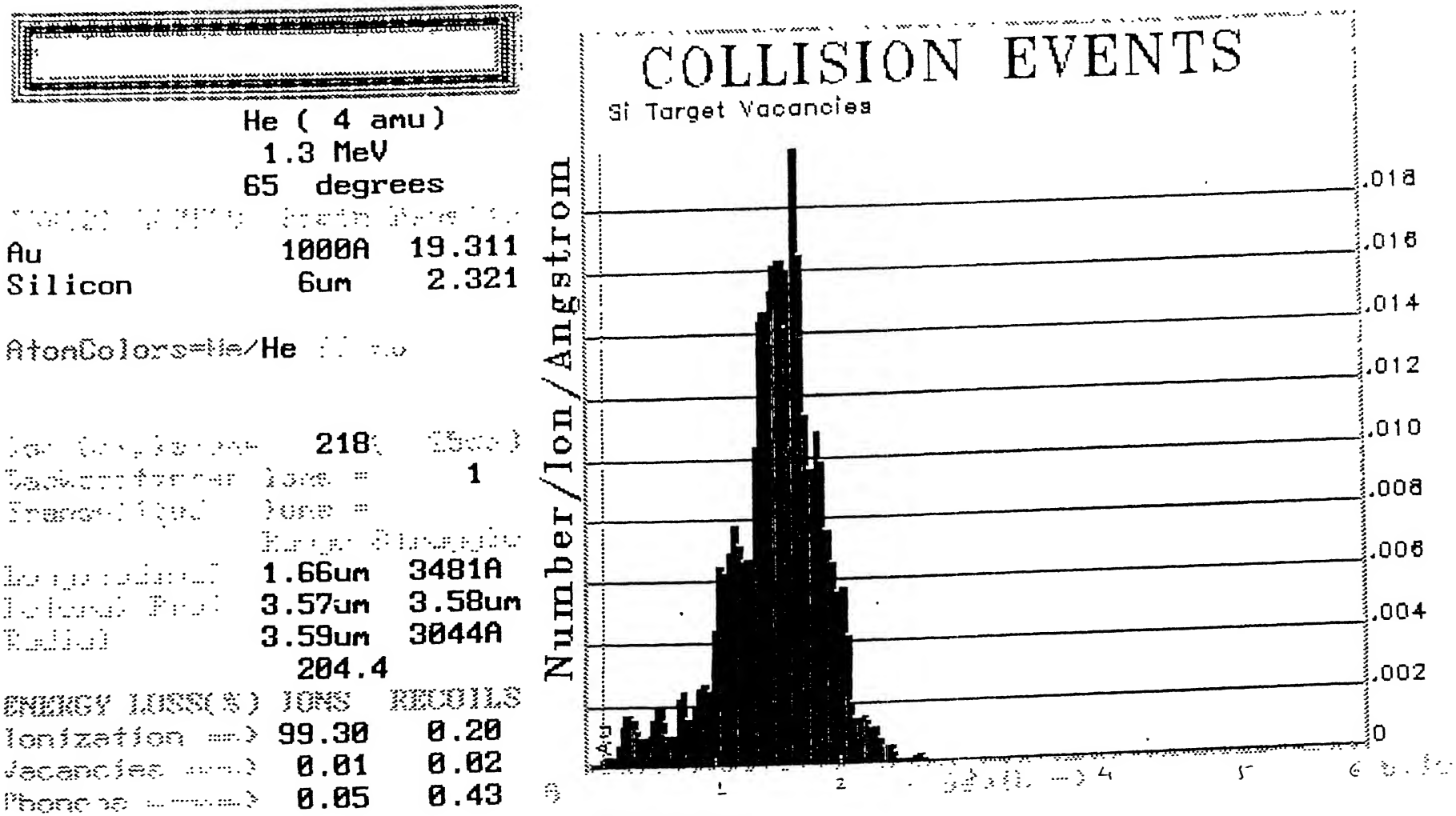

Fig.4.8 Vacancy Profile in Silicon induced by He^{+} Ions(1.3MeV,65^{0})

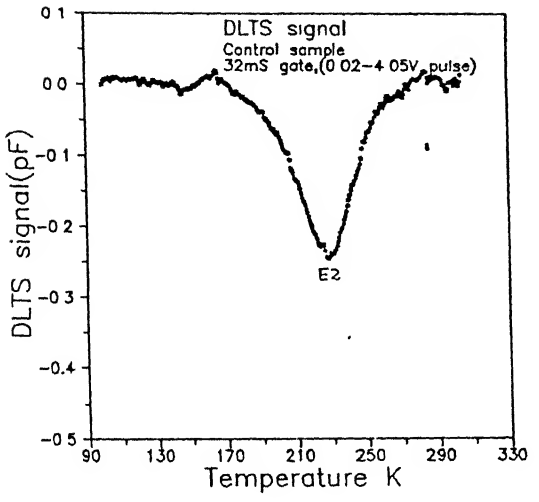

Fig. 4.9(a) DLTS curve for control sample.

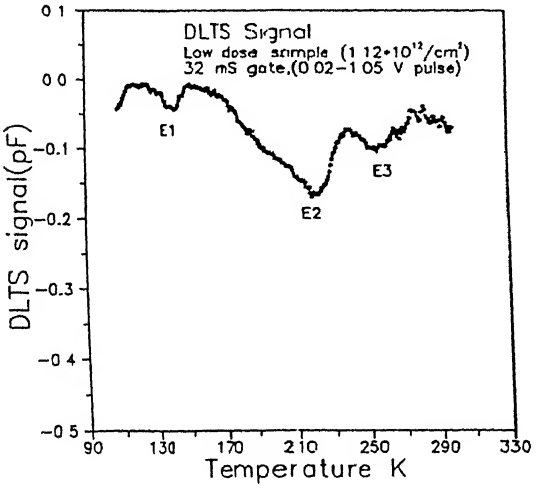

Fig. 4.9(b) DLTS curve for low dose sample.

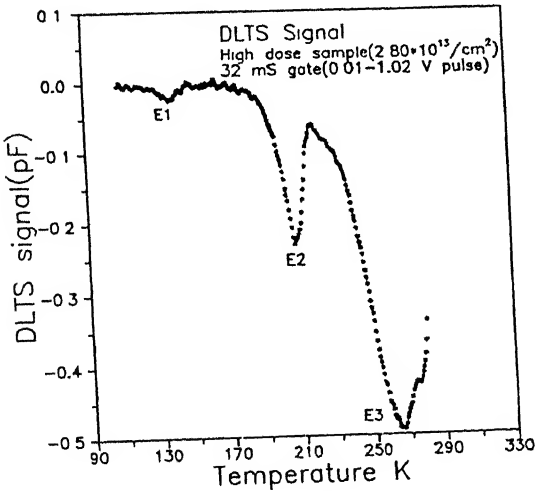

Fig. 4.9(c) DLTS curve for high dose sample.

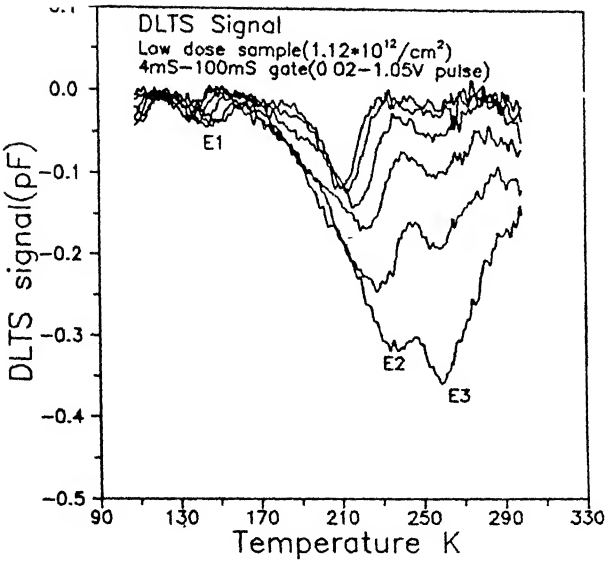

Fig. 4.10 DLTS curve for low dose sample for different gates.

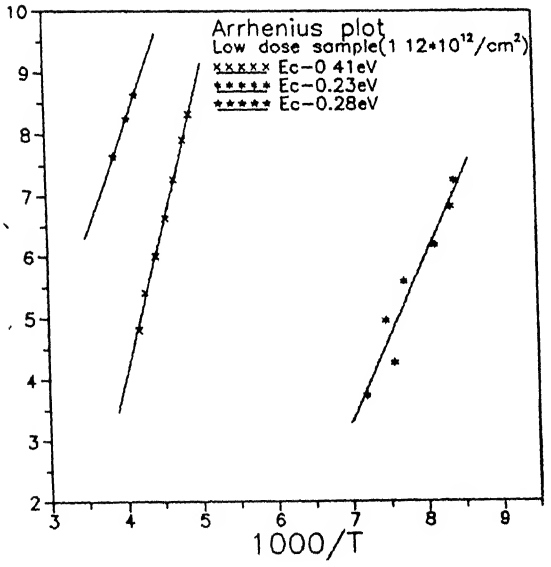

Fig. 4.11 Arrhenius plot for various levels in low dose sample.

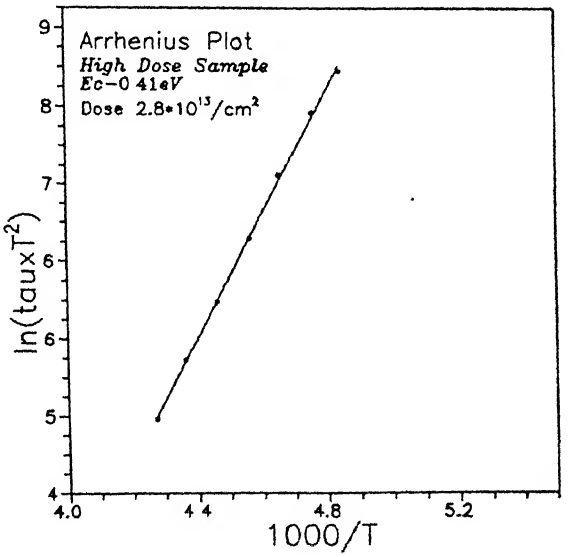

Fig. 4.12 Arrhenius plot for Ec-0.4 high dose sample.

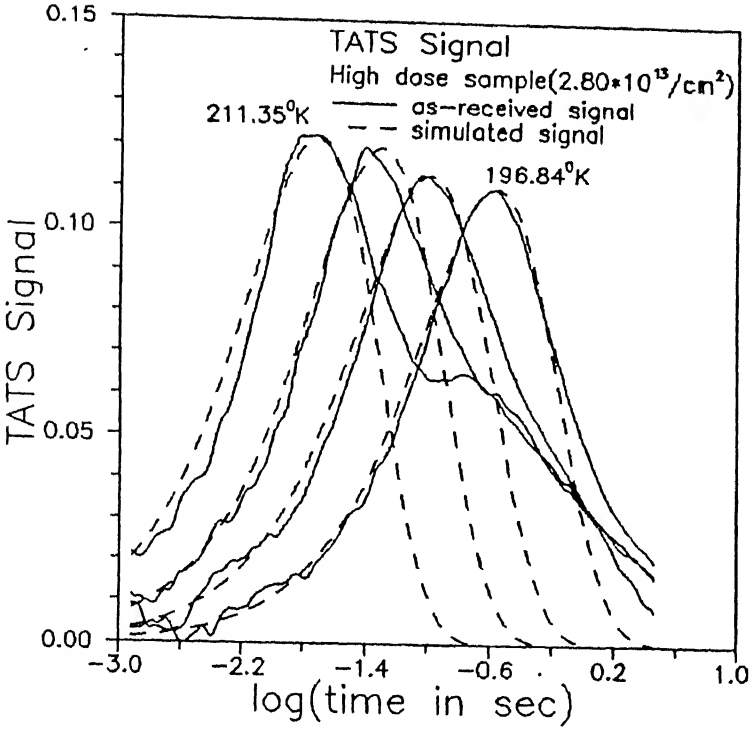

Fig 4.13 (a) TATS spectra for high dose sample at various temperarures.

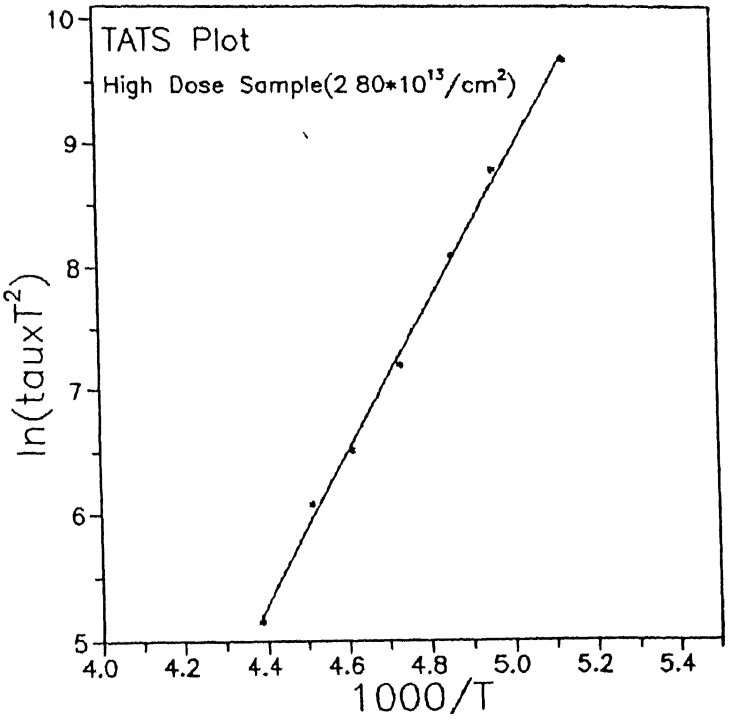

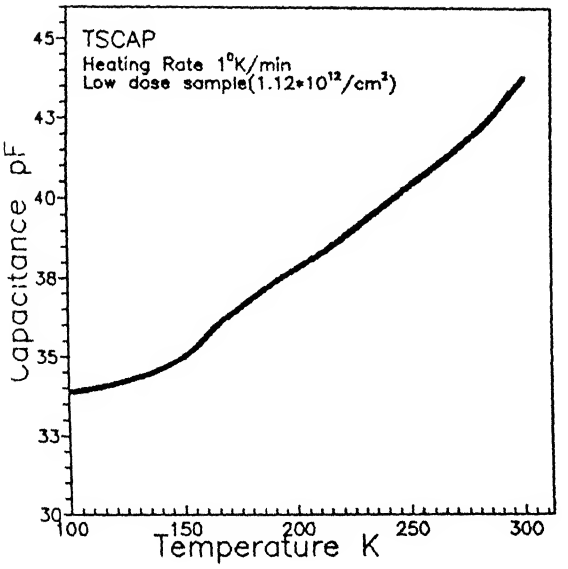

Fig. 4.14(a) TSCAP curve for low dose sample.

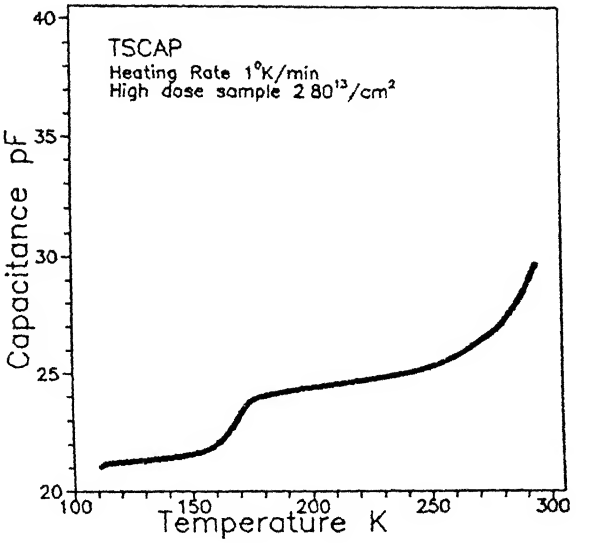

Fig. 4.14(b) TSCAP curve for high dose sample.

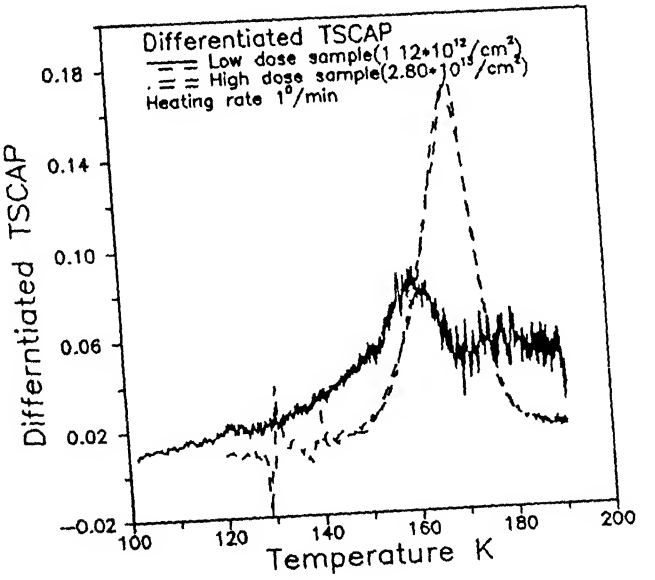

Fig. 4.15 Differentiated TSCAP curve for low and high dose sample.

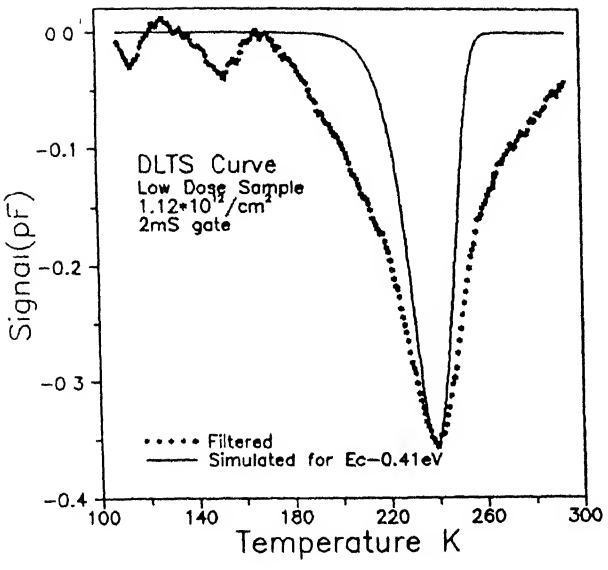

Fig. 4.16 Experimental and Simulated DLTS curve for Ec-0.41eV in low dose sample for 2 mS gate.

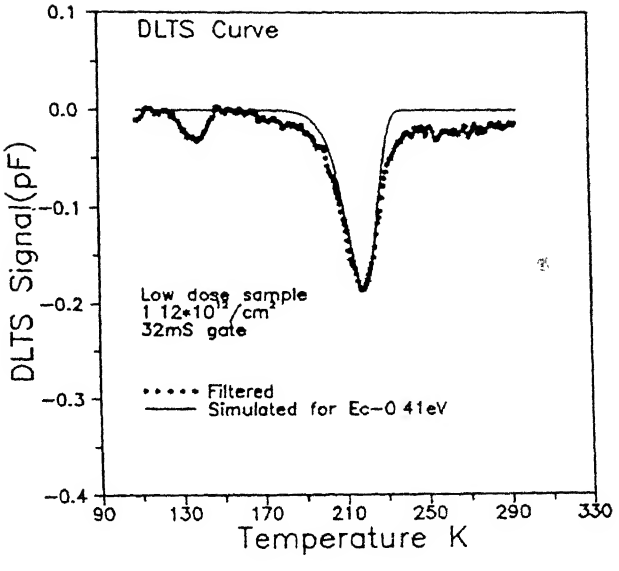

Fig. 4.17 Experimental and Simulated DLTS curve for Ec-0.41eV in low dose sample for 32 ms gate.

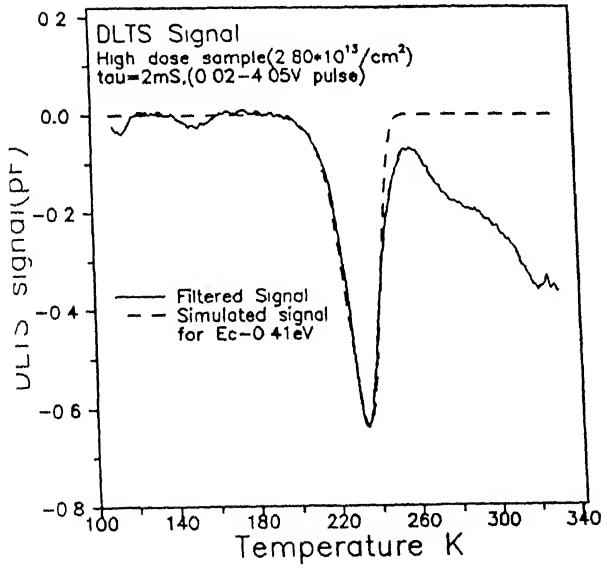

Fig. 4.18(a) Experimental and Simulated DLTS curve for Ec-0.41eV in high dose sample for 2ms gate.

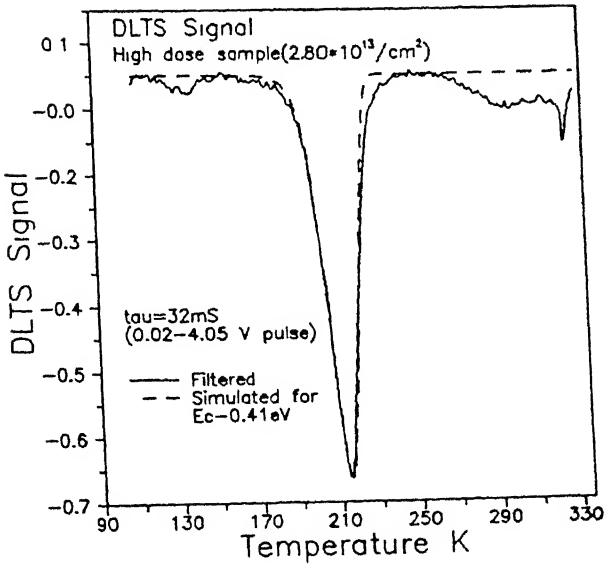

Fig. 4.18(b) Experimental and Simulated DLTS curve for Ec-0.41eV in high dose sample 32ms gate.

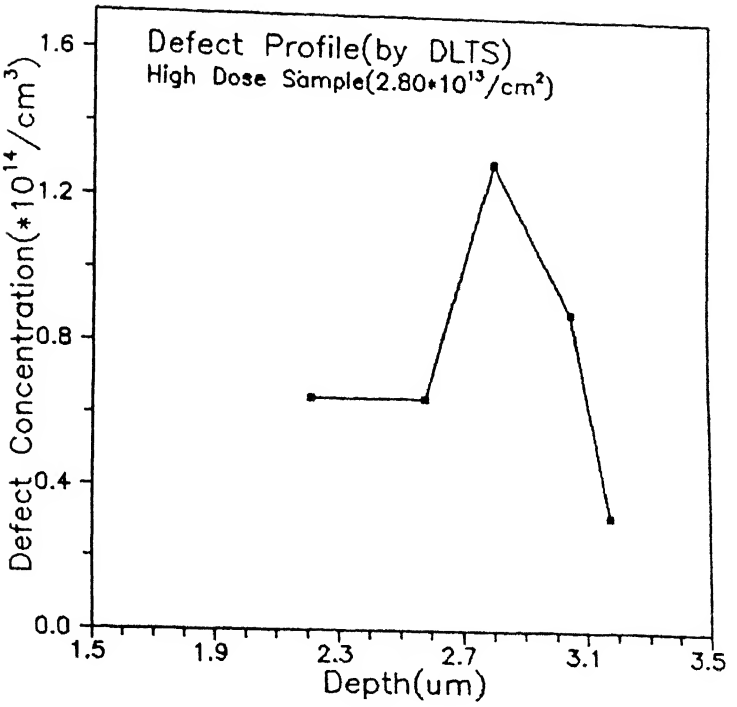

Fig. 4.19(a) Experimental defect profile of Ec-0.41eV by DLTS measurement in high dose sample.

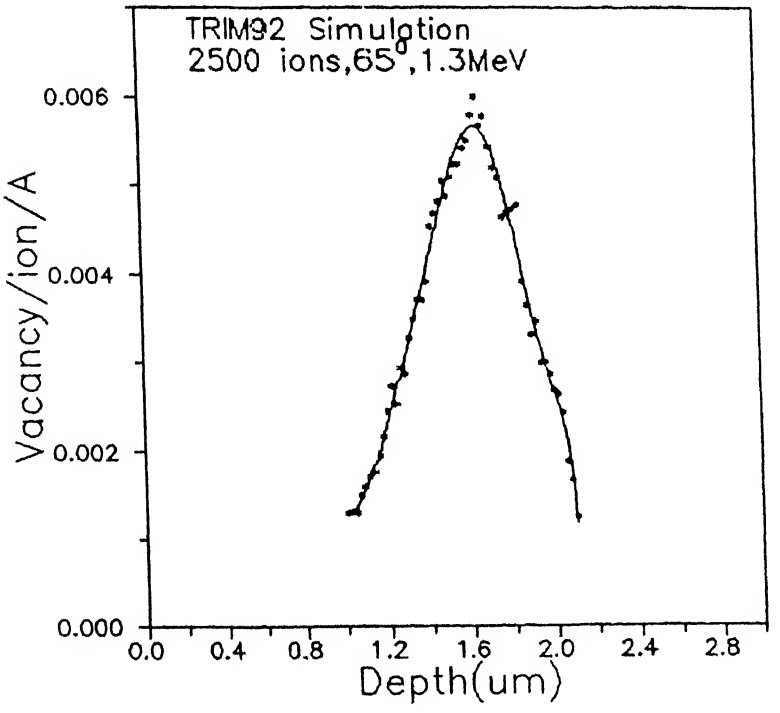

Fig. 4.19(b) Simulated vacancy profile for 2500 ions at 65°, 1.3MeV by TRIM92.

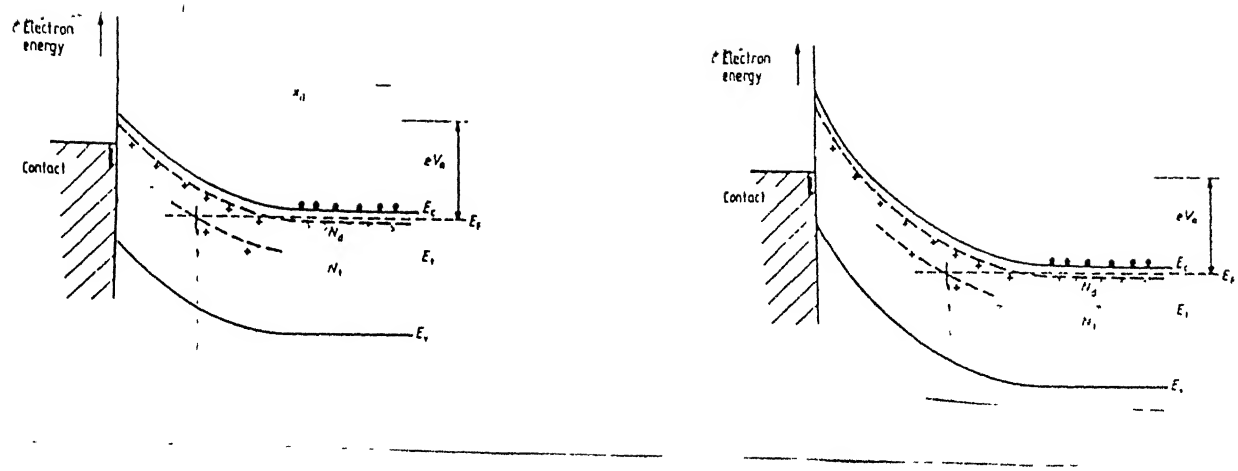

Fig. 4.20 Band bending diagram of n-type semiconductor showing E_F and E_T crossing for two diffrent bias.

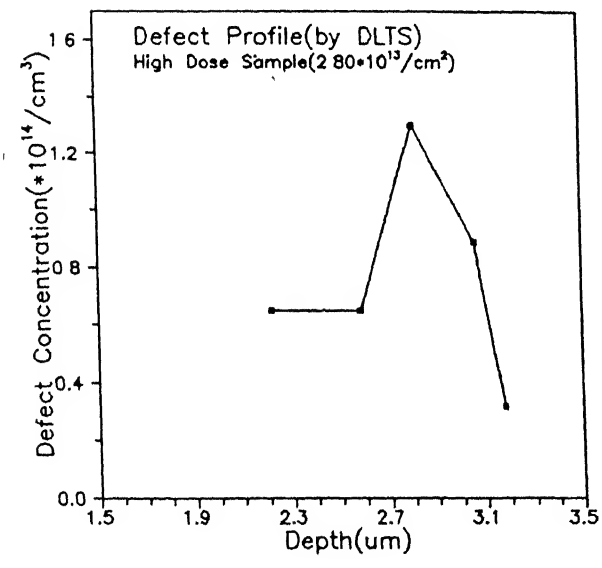

Fig 4 21(a) Experimental defect profile for E_t-0.41eV by DLTS Measurement in high dose sample.

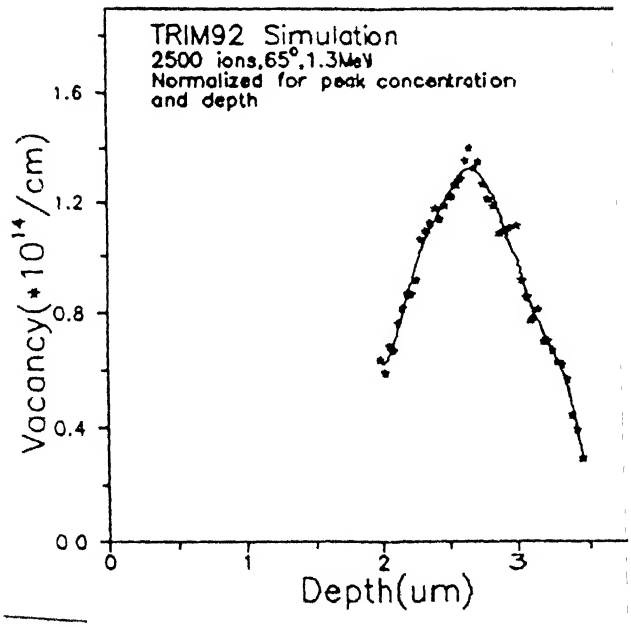

Fig. 4.21(b) Normalized peak concentratio and depth of simulated vacancy profile

Table 4.1

Angle	Ion Energy	Z_1	Z_2	E_d	E_b
0^0 or 65^0	1300 keV	4	14	13eV	1.5eV

Tab 4.1 Parameters used for TRIM92 simulation

Table 4.2

PEAK	Energy(eV)	Capture cross section $\sigma_{n(cm^2)}$	Identification
E1	Ec-0.23	$5.7x10^{-15}$	V-V(=/-)
E2	Ec-0.41	$3.3x10^{-15}$	V-V(-/0)+(P-V)
E3	Ec-0.28	$1.9x10^{-19}$	not related ?

Tab.4.2 Results obtained from DLTS study